

Paleoceanography and Paleoclimatology



RESEARCH ARTICLE

10.1029/2018PA003453

Key Points:

- Similar trends in $\text{TEX}_{86}^{\text{H}}$, Mg/Ca, and $\delta^{18}\text{O}$ records confirm that the fundamental processes underlying proxy relationships remained constant over time
- Benthic Mg/Ca appears to overestimate bottom water temperatures, possibly because the relation between seawater Mg/Ca and Mg incorporation is not linear
- The Bass River temperature record is similar to open ocean records, suggesting that the Bass River is predominantly responding to global climate change

Supporting Information:

- Supporting Information S1

Correspondence to:

M. W. de Bar,
marijke.de.bar@nioz.nl

Citation:

de Bar, M. W., de Nooijer, L. J., Schouten, S., Ziegler, M., Sluijs, A., & Reichart, G.-J. (2019). Comparing seawater temperature proxy records for the past 90 Myrs from the shallow shelf record Bass River, New Jersey. *Paleoceanography and Paleoclimatology*, 34, 455–475. <https://doi.org/10.1029/2018PA003453>

Received 10 AUG 2018

Accepted 27 FEB 2019



Accepted article online 4 MAR 2019

Published online 2 APR 2019

©2019. The Authors.

This is an open access article under the terms of the Creative Commons Attribution-NonCommercial-NoDerivs License, which permits use and distribution in any medium, provided the original work is properly cited, the use is non-commercial and no modifications or adaptations are made.

Comparing Seawater Temperature Proxy Records for the Past 90 Myrs From the Shallow Shelf Record Bass River, New Jersey

M. W. de Bar¹, L. J. de Nooijer¹, S. Schouten^{1,2}, M. Ziegler², A. Sluijs² , and G.-J. Reichart^{1,2} 

¹NIOZ Royal Netherlands Institute for Sea Research, and Utrecht University, Den Burg, Texel, The Netherlands,

²Department of Earth Sciences, Faculty of Geosciences, Utrecht University, Utrecht, The Netherlands

Abstract We present a multiproxy (foraminifer Mg/Ca, $\delta^{18}\text{O}$, Δ_{47} , and Sr/Ca, and biomarker $\text{TEX}_{86}^{\text{H}}$, MAT_{mrs}) low-resolution paleotemperature record based on seven sets of high-resolution time series from the late Cretaceous to Miocene from the Ocean Drilling Program Bass River site, New Jersey Shelf, North Atlantic. Along with insight into long-term climate evolution, this allows testing for internal consistency between proxies. The bottom water temperatures (BWTs) reconstructed using benthic $\delta^{18}\text{O}$ and Mg/Ca values show good agreement in recorded trends with the $\text{TEX}_{86}^{\text{H}}$ sea surface and shallow subsurface temperature record, and with the stacked global benthic oxygen isotope record. The Mg/Ca-based BWTs are higher than the $\delta^{18}\text{O}$ -based BWTs, likely due to uncertainty in the assumptions associated with the Mg/Ca calibration to seawater Mg/Ca. Absolute $\delta^{18}\text{O}$ -based BWT reconstructions are supported by clumped isotope paleothermometry. The agreement in main trends of the independent paleotemperature proxies indicates that the underlying assumed mechanisms for the different proxy relations to temperature stayed largely intact back to at least 90 Ma. Consistent differences in absolute temperature values highlight, however, that a better understanding of the individual proxies is required in order to achieve accurate absolute temperature reconstructions

1. Introduction

Over the last 100 million years, Earth's climate has undergone major changes on long and short time scales (Friedrich et al., 2012; Zachos et al., 2008). The Late Cretaceous to early Eocene was generally characterized by warm climates and high CO_2 concentrations and is referred to as the “greenhouse world” (e.g., Anagnostou et al., 2016; Bijl et al., 2009; Cramwinckel et al., 2018; Foster et al., 2017; O'Brien et al., 2017). A subsequent long-term drop in temperature and CO_2 during the late Cenozoic resulted in colder, glaciated conditions often termed the “icehouse” (e.g., Anagnostou et al., 2016; Cramwinckel et al., 2018; Miller et al., 1991; Zachos et al., 2008). Underlying such conclusions are geochemical and paleontological proxies to reconstruct individual environmental parameters. Seawater temperature can be reconstructed by a number of proxies, based on organic compound distributions, elements, and isotopes incorporated in calcitic fossils and relative abundances of species of specific genera. However, every proxy has limitations, and many have been shown to depend on other parameters beside seawater temperature (e.g., Elderfield et al., 2002; Norris et al., 2002). Consequently, it may be uncertain whether recorded patterns solely reflect changes in temperature or whether they are biased by trends in other environmental or geochemical parameters.

Application of proxies in deep time can be particularly affected by increasing deviation from present-day conditions, which potentially compromises calibrations using present-day relations. For example, foraminiferal Mg/Ca can be used to reconstruct past temperatures (Nürnberg et al., 1996; Rosenthal et al., 1997) but is also influenced by seawater Mg/Ca ($\text{Mg}/\text{Ca}_{\text{sw}}$; Delaney et al., 1985; Segev & Erez, 2006). Although this method is quite robust for the recent past due to the relatively long residence times of Ca^{2+} and Mg^{2+} in the ocean, Mg/Ca-based temperatures become increasingly inaccurate in deep time. A number of low-resolution geochemical models have estimated past seawater $[\text{Mg}^{2+}]/[\text{Ca}^{2+}]$ (e.g., Berner, 2004; Farkas et al., 2007; Stanley & Hardie, 1998), showing that this ratio varied between ~ 1 and ~ 5 mol/mol during the Phanerozoic, with a potentially major impact on Mg/Ca-based temperature reconstructions. These models have been crosschecked using fluid inclusions in halite (Horita et al., 2002; Lowenstein et al., 2001), analysis of ridge flank vein carbonates (Coggon et al., 2010), by comparing Mg/Ca ratios of fossil and modern echinoderms (Dickson, 2004), Mg/Ca ratios of different foraminiferal

species (Wit et al., 2017), and by combining Mg/Ca and with clumped isotope analysis in large benthic foraminifera (Evans et al., 2018).

Similarly, the oxygen isotopic composition of seawater varied globally over geological time, and also, local variations form a major complication in reconstructing paleotemperatures based on $\delta^{18}\text{O}$ of foraminiferal shells. For this reason, clumped isotope (Δ_{47}) thermometry complements $\delta^{18}\text{O}$ records, as this proxy is independent of the $\delta^{18}\text{O}$ of the seawater (Eiler, 2007). The Δ_{47} thermometer is based on the “clumping,” that is, ordering, of the ^{13}C and ^{18}O isotopes in a carbonate ion, which is a function of the temperature at which the calcite precipitated. The disadvantage of the clumped isotope method is its relatively low precision, which requires a large number of replicate analysis and large sample sizes, making it currently not a feasible proxy for high-resolution reconstructions, despite recent progress in analytical techniques (Fernandez et al., 2017; Meckler et al., 2014; Müller et al., 2017). The Sr/Ca ratio of foraminifera also correlates to seawater temperatures (e.g., Elderfield et al., 2000; Lea et al., 1999; Rathburn & DeDeckker, 1997; Reichart et al., 2003; Rosenthal et al., 2006), although application of Sr/Ca as a temperature proxy is complicated by the effects of growth rates, salinity, seawater Sr/Ca, and pH (Kisakürek et al., 2008; Lea et al., 1999), as well as seawater carbonate chemistry (e.g., Dissard et al., 2010; Dueñas-Bohórquez et al., 2009; Dueñas-Bohórquez et al., 2011; Keul et al., 2017; Raitzsch et al., 2010; Russell et al., 2004). In addition to the foraminifera-based proxies, organic proxies, based on relative abundances of biomarker molecules, are regularly applied in paleoclimate studies. Organic proxies are not significantly influenced by the elemental and isotopic composition of seawater. One of the most established sea surface temperature (SST) proxies is $U^{K'}_{37}$, which is based on the degree of unsaturation of alkenones (Brassell et al., 1986). However, temperature reconstructions based on alkenones are limited to the last ~55 Myrs because triunsaturated alkenones are absent in older sediments (Brassell, 2014, and references therein). Moreover, the proxy becomes increasingly unreliable at higher temperatures since the index reaches its upper limit at 28 °C (e.g., Conte et al., 2006). However, recently, Tierney and Tingley (2018) developed a new Bayesian regression calibration model for the $U^{K'}_{37}$ and observed a substantial attenuation of the $U^{K'}_{37}$ response to temperature at temperatures above 24 °C, with the index approaching unity at a SST of around 29.6 °C. Another widely applied SST proxy is the TEX_{86} index, based on isoprenoidal glyceryl dialkyl glyceryl tetraethers (GDGTs), which in the marine environment are mainly derived from Thaumarchaeota (Kim et al., 2010; Schouten et al., 2002). However, it has been shown that this proxy might (regionally) reflect subsurface temperatures rather than SST (Chen et al., 2014; Huguet et al., 2007; Kim et al., 2012; Kim et al., 2015; Lopes dos Santos et al., 2010; Schouten et al., 2013). Moreover, the proxy may regionally be biased by changes in seawater ammonia and oxygen concentrations (e.g., Hurley et al., 2016; Qin et al., 2014, 2015). Culture studies have shown that growth phase may also markedly influence the GDGT composition (Elling et al., 2014), whereas salinity and pH changes have a minor impact only on the lipid composition (Elling et al., 2015; Wuchter et al., 2004). Finally, there is discussion how to calibrate TEX_{86} indices to temperature outside the range of the modern core top calibration; particularly, at the warm end the assumption of an asymptotic or linear relation between SST and TEX_{86} leads to a difference of several degree celsius (e.g., Cramwinckel et al., 2018; Tierney & Tingley, 2014).

Proxies for continental temperature are typically also based on carbonate and organic biogenic sediment components. Along with $\delta^{18}\text{O}$ and clumped isotope thermometry (e.g., Snell et al., 2013), Cretaceous and Paleogene temperature reconstructions are based on leaf assemblages (e.g., Wing et al., 2005) and biomarkers (e.g., Sluijs et al., 2014; Weijers et al., 2007). The biomarker-based proxy, MAT_{mrs} , is based on GDGTs produced by soil bacteria (de Jonge et al., 2014; Peterse et al., 2012; Weijers et al., 2007) and often applied on nearshore marine deposits. However, in situ production might compromise the proxy regionally (Liu et al., 2014; Peterse et al., 2009; Sinninghe Damsté, 2016).

Because the uncertainties and biases are proxy specific, reconstructions of absolute SSTs are ideally based on multiple proxies applied to the same samples, to test for consistency (e.g., Frieling et al., 2017; Lopes dos Santos et al., 2010). Indeed, the different inherent complications for the individual proxies call for an integrated, multiproxy approach, in which temperature records are intercalibrated. Such an approach addresses underlying assumptions and may reveal potential limitations and pitfalls of the individual proxies. Also, as these proxies are primarily based on empirical calibrations, it remains to be established whether the fundamental processes underlying the proxy relationships remain intact also in deep time.

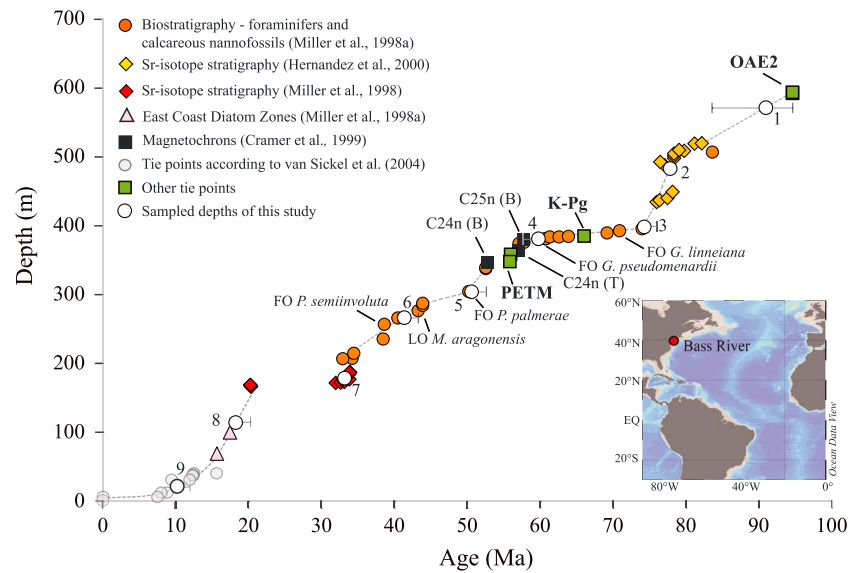


Figure 1. The reconstructed age model for the Bass River core. The orange dots reflect biostratigraphic ages (Miller, Sugarman, et al., 1998); the black squares are magnetostratigraphic tie points (Cramer et al., 1999). Sr-isotope data are displayed as yellow (Hernandez & Feigenson, 2000) and red diamonds (Miller, Sugarman, et al., 1998). The two pink triangles reflect the base and top of East Coast Diatom Zone 2 recognized by Miller, Sugarman, et al. (1998). The other tie points are described in section 2. The transparent gray dots (0–16 Ma) are sequence unconformity (Miller, Sugarman, et al., 1998) ages reported in van Sickle et al. (2004), tied to the Gradstein et al. (1995) time scale. The sediments sampled in this study are plotted as white dots with error bars reflecting the maximum age uncertainty, that is, the “distance” to the nearest age tie points. LO = last occurrence; FO = first occurrence; B = base; T = top; OAE2 = Ocean Anoxic Event 2; PETM = Paleocene Eocene thermal maximum. In the bottom right corner we show the site location, as created in Ocean Data View (Schlitzer, 2015).

Numerous studies have assessed changes in climate throughout the Cretaceous and Paleogene from seawater temperature reconstructions using single-proxy, twin-proxy, or multiproxy approaches (e.g., Burgess et al., 2008; Forster et al., 2007; Frieling et al., 2017; Hollis et al., 2012), particularly comparing TEX_{86} and planktonic foraminiferal $\delta^{18}O$ and Mg/Ca . These multiproxy reconstructions focus on particular (extreme) climate events/transitions, where certain assumptions underlying the temperature proxies or preservation of the proxy carriers in question may not hold true or local climate conditions can be of major influence. A more general long-term multiproxy temperature intercomparison on well-preserved fossils from one single site allows validation of the different proxies used and evaluation of the validity of the underlying presumed proxy relationships. Due to scarcity of sites suited for both organic and inorganic proxies, there are only a few long-term (>Myrs) paleotemperature studies from a single site (e.g., Hollis et al., 2012; Pearson et al., 2007). Hence, past long-term changes in seawater temperature are currently inferred from the stacked deep-sea benthic foraminiferal oxygen isotope record (Friedrich et al., 2012; Zachos et al., 2008), based on combined records from Deep Sea Drilling Project and Ocean Drilling Program sites. Although this has the fundamental advantage of best representing a global average, such an approach is not suited for comparing different proxies.

Here we apply a multiproxy approach using foraminiferal calcite and organic proxies to generate a low-resolution, long-term (90 Myr) paleotemperature record for northeast America, based on the Bass River site (New Jersey, North Atlantic). Benthic and planktonic foraminiferal oxygen isotopes, clumped isotopes, and foraminiferal shell Mg/Ca and Sr/Ca values, as well as the TEX_{86} and MAT_{mrs} , were determined on material from the same core, and all used to independently assess seawater and air temperatures.

2. Materials and Methods

2.1. Site Description

A total of 596.34 m (1,956.5 ft) of sediment section was drilled at the Bass River site (39°36′42″N, 74°26′12″W) during Ocean Drilling Program Leg 174AX on the New Jersey Coastal Plain (see map in Figure 1; Miller

et al., 1998). The current-day average annual air temperature is approximately 12.4 °C, with seasonal maxima of around 17.7 °C and minima of around 7.1 °C, as derived from data covering 1981 to 2010 (Atlantic City, New Jersey; U.S. Climate Data, 2017; <https://www.usclimatedata.com/>). Castelao et al. (2010) monitored temperature and salinity along multiple hydrographic profiles by means of glider observations over 4 years and showed that during winter months, shelf waters are vertically homogeneous in temperature (5–10 °C). Around May, a shallow thermocline develops, reaching maximum intensity in August. In this period, surface temperatures vary between 20 and 25 °C, with a thermocline depth of approximately 10 to 15 m and coinciding bottom water temperatures (BWTs) of ~10 °C (see Figure 2 in Castelao et al., 2010).

The Bass River site covers strata from the Cenomanian to the Holocene (Miller, Sugarman, et al., 1998). The recovered siliciclastic sediments (sands, silts, and clays), with some biogenic carbonate and organic matter, were deposited in a neritic setting. Microfossil and sedimentological data indicate that regional sea level varied across the studied interval so that the setting varied between very shallow marine to outer shelf settings (e.g., Miller et al., 1998). Sediments were generally deposited below storm wave base and temperature reconstructions based on mixed layer, and benthic organisms indicate the sustained presence of a thermocline (e.g., John et al., 2008; Miller, Sugarman, et al., 1998). Detailed description of the core in terms of sedimentary textures, structures, colors, fossil content, lithostratigraphic units, lithological contacts, and sequences is provided by the site report of Miller, Sugarman, et al. (1998).

We updated the original age model of the entire section (Miller, Sugarman, et al., 1998) using the most recent tie points based on strontium (Sr) and carbon isotope stratigraphy, biostratigraphy (nannofossils, foraminifera, dinoflagellates, and diatoms), and magnetostratigraphy. Among others, analyses at Bass River resulted in the identification of Oceanic Anoxic Event 2, the Cretaceous-Paleogene boundary event, and the Paleocene-Eocene Thermal Maximum (Cramer et al., 1999; Hernandez & Feigenson, 2000; Olsson et al., 2002; Sugarman et al., 1999; van Helmond et al., 2016). All biostratigraphic and magnetostratigraphic ages were assigned an age following the Gradstein et al. (2012) time scale. Also, the Sr-isotope data from Miller, Sugarman, et al. (1998) and Hernandez and Feigenson (2000) were updated to the Geological Timescale 2012 (Gradstein et al., 2012). However, we deduced the ages from Figure 7.2 of Gradstein et al. (2012; chapter 7), showing the world's ocean $^{87}\text{Sr}/^{86}\text{Sr}$ variation through time, and thus, uncertainties are relatively large (± 2.5 Myr). Due to sparse chronostratigraphy for the youngest part of the core (last ~15 Ma), we adapted some tie points from van Sickle et al. (2004), which are tied to the Gradstein et al. (1995) time scale, for which van Sickle et al. (2004) reported a typical age uncertainty of ± 0.5 Myr. The two pink triangles (Figure 1) reflect the base and top of East Coast Diatom Zone 2 recognized by Miller, Mountain, et al. (1998). The zonation was developed by Andrews (1988), and by comparing the position of East Coast Diatom Zone 2 to overlapping Planktonic Foraminifera Zones (following Blow, 1969), we have assigned absolute ages using the Geological Timescale of Gradstein et al. (2012). Although the uncertainties are rather large, this is sufficient for the purposes of our study.

2.2. Sample Strategy and Dating

In order to reconstruct past long-term seawater temperature evolution, we sampled nine sediment intervals across the Late Cretaceous to the Late Miocene. For every sample interval, we took 10 or 11 subsamples (95 samples in total), spanning depth intervals ranging between ~0.5 and 5.5 m (see Table S1 in the supporting information for a list of all samples). This approach implies that short-term variability such as Milankovitch cyclicity is captured within the high-resolution data sets underlying the longer-term low-resolution data. Our estimates of SST for the time slices spanning more than 100 kyrs therefore effectively average out most shorter term variability related to orbital forcing. However, our initial age model was tied to the Gradstein et al. (1995) time scale, and updating all stratigraphic tie points to the Gradstein et al. (2012) time scale changed the assigned ages, as well as the time captured within the intervals sampled, which eventually range between ~30 and 900 kyr.

Individual sample ages were based on linear regressions fitted through nearby age tie points of the updated age model (Figure 1), with exception of sample interval 9, which was dated based on an exponential fit, as an exponential function was the best fit for the ages of van Sickle et al. (2004).

The oldest sediments sampled (sample interval 1) were recovered from between ~572- and 568-m depth in the Bass River Formation. At 518 m, the lowermost constraints based on Sr-isotopes indicate an age of

~82 Ma (± 2.5 Myr). Additionally, two tie points at ~592 m, representing the onset of the carbon isotope excursion associated with Ocean Anoxic Event 2, indicate an age of 94.64 (± 0.12 Ma); Bowman & Bralower, 2005; Eldrett et al., 2015; Sugarman et al., 1999; van Helmond et al., 2014) and the first consistent presence of the dinocyst morphological complex *Cyclonephelium compactum-membraniphorum* during the Plenus Cold Event (van Helmond et al., 2016), which is ~10 kyr younger. We assumed constant sedimentation rates between these two oldest age tie points and the oldest Sr-isotopic age, resulting in an age of ~90.9 Ma for sample interval 1, but with large maximum uncertainty of ± 8.7 Myrs based on the largest “distance” to the closest age tie points (Figure 1). Interval 1 covers hence a ~700-kyr time interval (gray dashed line; Figure 1).

Sample intervals 2 and 3 are positioned between ~482- and 481-m (Woodbury Formation) and 397- and 396-m depth (Mont Laurel Formation), respectively, and were dated at ~77.8 (± 0.6 , although surrounding Sr-isotope tie points have uncertainties of ± 2.5 Myrs) and ~74.1 (± 1.9) Ma, covering ~30 and 40 kyrs, respectively. Interval 4 was sampled at a depth between ~380 and 379 m (Mount Laurel Formation), which is just above the position of Cretaceous-Paleogene (K-Pg) boundary at ~384-m depth (66.04 [± 0.05] Ma; Olsson et al., 2002). The linear interpolation between several biostratigraphic, magnetostratigraphic, and the K-Pg age tie point in this part of the core implies an age of ~60.1 (± 2.4) Ma, the interval covering ~800 kyrs. Samples for interval 5 were taken in between ~305- and 303-m depth, from the Manasquan Formation. Age assessment of this interval was established using the first occurrence of *Planorotalites palmerae* at 303.6 m, defining the base of planktonic foraminiferal Zone P9 (Miller, Sugarman, et al., 1998), and surrounding biostratigraphic tie points. The assumption of constant sedimentation rates between these tie points results in an age of ~50.2 (± 2.3) Ma for sample interval 5, covering ~300 kyrs. The sediments of sample intervals 6 (~265- to 264-m depth, Shark River Formation) and 7 (~180- to 174-m depth, Atlantic City Formation) were dated at ~41.2 (± 2.1) and 33.4 (± 0.5 ; although surrounding Sr-isotope tie points have uncertainties of ± 2.5 Myrs) Ma, covering ~80 and 900 kyrs, respectively, based on the linear regressions. Age control for interval 8 (~116- to 111-m depth; Kirkwood Formation) is limited to diatom biostratigraphy (uncertainty ± 1 Myr) and Sr-isotopic ages (uncertainty ± 2.5 Myr) (Figure 1) and leads to an estimated age of 17.7 (± 2.5) Ma, the sampled interval covering ~200 kyrs. Age control for the sediments of interval 9 (~24–21 m) is very limited, and therefore, the sequence bounding unconformities were used (originally identified by Miller, Sugarman, et al., 1998) in combination with assigned ages as reported in van Sickle et al. (2004) (Figure 1; transparent dots), which are tied to the Gradstein et al. (1995) time scale. We fitted an exponential trend through these tie points, based on which the youngest sediments were dated, resulting in the age of 10.7 (± 1.3) Ma, covering ~700 kyrs.

2.3. Foraminiferal Geochemistry

In this study, BWTs were derived from benthic foraminiferal shell geochemistry. Planktonic foraminifera were generally less abundant throughout the core, due to the shallow paleodepth of the site (e.g., Miller, Sugarman, et al., 1998). Only the sediment interval of 50 Ma contains relatively high numbers of planktonic foraminifera, agreeing with the relative high eustatic sea level at this time, resulting in outer neritic conditions at Bass River (e.g., Miller, Sugarman, et al., 1998; Miller et al., 2005; van Sickle et al., 2004). Also, the age intervals of 60 and 41 Ma contain somewhat more planktonic foraminifera. The sediments of the time slices of 33, 74, 78, and 91 Ma contain few planktonic foraminifera, and the two youngest intervals are barren of foraminifera. We combined planktonic specimens for the age intervals of 41, 50, and 60 Ma, respectively, to obtain an average planktonic oxygen isotope value per age interval. For the interval of 41 Ma, we measured the average $\delta^{18}\text{O}$ (and $\delta^{13}\text{C}$) for the species *Acarinina collactea*, *A. pseudotopilensis*, and *Parasubbotina varianta* (Figure S2). For the sediments of 50 Ma, we obtained an average $\delta^{18}\text{O}$ value for *Subbotina* spp., and for the time slice of 60 Ma, we analyzed *S. velascoensis*. For *S. velascoensis*, we picked enough specimens for four measurements, whereas for the other species/genera we performed one analysis only. Because of the limited availability of planktonic foraminifera over the long time scale considered here, we chose to establish Mg/Ca (or Sr/Ca in case of aragonitic species) and $\delta^{18}\text{O}$ records for all age intervals based on benthic foraminifera, as these are abundant throughout the core except near the top.

The main benthic foraminiferal genera found throughout the core are *Bulimina*, *Osangularia*, *Gyroidinoides*, *Anomalinoides*, *Gavelinella*, *Lenticulina*, *Cibicidoides*, and *Epistomina*. Single specimens of species within the genera *Cibicidoides*, *Gavelinella*, *Epistomina* (aragonitic), and *Lenticulina* spp. were handpicked for

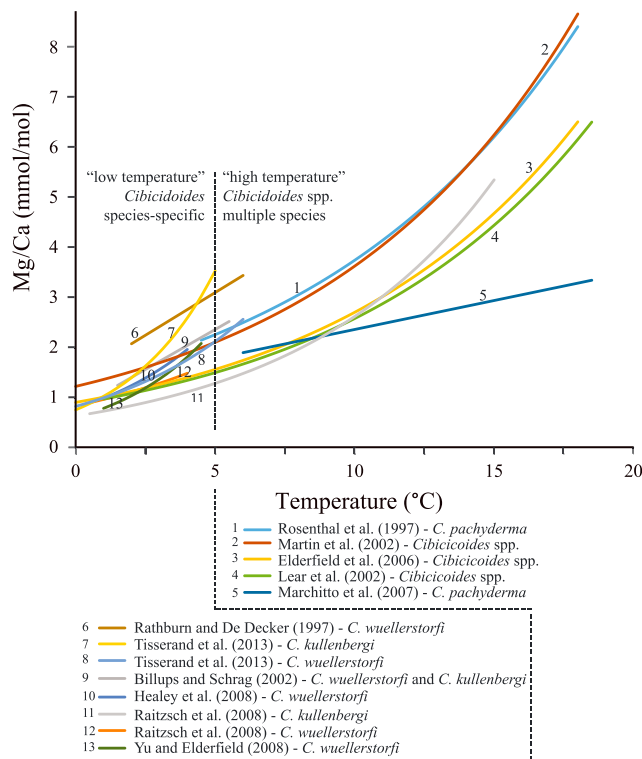


Figure 2. Mg/Ca calibrations for species-specific or multiple species *Cibicidoides* spp. The dotted line reflects the distinction between the low temperature calibrations (6–13) often based on a single species and the high temperature calibrations based on multiple species or on *C. pachyderma* (1–5). For our deep-time reconstruction we apply the calibration of Martin et al. (2002) and Lear et al. (2002) (2 and 4).

geochemical analysis. *Cibicidoides* showed highest abundances throughout the core and is often used in paleoenvironmental studies, as it is considered a trustworthy recorder of bottom water conditions (e.g., Marchitto et al., 2007). It has a global occurrence throughout many Paleogene sequences, and therefore, it has also been analyzed in the intervals of ~33, 41, 50, 60, and 74 Ma. The two youngest intervals (i.e., 11 and 18 Ma) did not contain foraminifer shells, and thus, we were not able to determine foraminiferal Mg/Ca and $\delta^{18}\text{O}$ for these ages. The interval at ~78 Ma contained very little foraminiferal specimens and those that were present belonged almost exclusively to the genus *Lenticulina*, which although not often applied in paleo-studies, were therefore used for this interval. Samples at ~91 Ma were dominated by *Gavelinella* spp. and the aragonitic *Epistomina* spp., which were picked here for analysis. *Gavelinella* specimens were also picked for the ~74-Ma interval, allowing intercomparison of the Mg/Ca- and $\delta^{18}\text{O}$ -based temperature estimates between *Gavelinella* and *Cibicidoides*.

Foraminifera were obtained by washing and sieving bulk marine sediment into two different size fractions (100–250 and >250 μm). Specimens larger than 250 μm were selected for geochemical analyses, and only in few cases when insufficient numbers of large specimens were available, smaller specimens were used. Prior to analyses, all foraminiferal tests were cleaned to remove adhering clay and other detrital material by rinsing with ethanol and ultrasonication, repeatedly pipetting off the supernatant. Visual examination and scanning electron microscopy indicated that preservation of foraminifers was generally good (Figures S1 and S2). Moreover, determined calcitic Al, Mn, and Mg concentrations (determined for the benthics only) were generally low (<65, 1, and 20 mmol/mol, respectively), which would not be the case after diagenetic alteration. For foraminiferal analyses, each subsample contained generally 10 benthic specimens. In total, 794 specimens have been analyzed

individually for Mg/Ca by means of laser ablation inductively coupled plasma mass spectrometry (LA-ICP-MS). Specimens were subsequently combined for oxygen isotopes resulting in 61 analyses (in some intervals foraminiferal assemblages were too sparse), using the same specimens as used for the laser ablation ICP-MS Mg/Ca analyses. Sediments have been extracted and analyzed for biomarker-based proxies for all 95 subsamples.

For the age intervals of 60 and 50 Ma, we combined 23 replicate measurements per time slice (mixed benthos) for clumped isotope analysis, in order to obtain an average Δ_{47} -derived BWT for the respective time intervals. A detailed description of the methods is included in the supplementary material.

2.4. Calculations of Temperatures Based on Proxy Values

2.4.1. Mg/Ca and Sr/Ca Calibrations

A large number of Mg/Ca-BWT calibrations for *Cibicidoides* spp. have been proposed (e.g., Billups & Schrag, 2002; Elderfield et al., 2006; Healey et al., 2008; Lear et al., 2002; Marchitto et al., 2007; Martin et al., 2002; Raitsch et al., 2008; Rathburn & DeDecker, 1997; Rosenthal et al., 1997; Tisserand et al., 2013; Yu & Elderfield, 2008; Figure 2; see Tisserand et al., 2013 for overview). The first Mg/Ca-T calibration for *Cibicidoides* from Rosenthal et al. (1997) spanned a temperature range from 4.5 to 18 °C, which was more recently extended by calibration studies using specimens collected from the deep sea, reaching somewhat lower temperatures (0–6 °C; e.g., Healey et al., 2008; Raitsch et al., 2008; Tisserand et al., 2013; Yu & Elderfield, 2008) and with calibrations covering temperatures up to 18 °C (Elderfield et al., 2006; Lear et al., 2002; Marchitto et al., 2007; Martin et al., 2002). Whereas the “high temperature” calibrations are based on multiple species of *Cibicidoides* (Elderfield et al., 2006; Lear et al., 2002; Martin et al., 2002) or on *C. pachyderma* (Marchitto et al., 2007; Rosenthal et al., 1997), calibrations with temperature ranges between 0 and 6 °C are based on species-specific analyses, most of which are based on *C. wuellerstorfi* or *C. kullenbergi*

(e.g., Billups & Schrag, 2002; Healey et al., 2008; Raitzsch et al., 2008; Yu & Elderfield, 2008). The species-specific “low temperature” calibrations show a higher temperature sensitivity (e.g., Healey et al., 2008; Yu & Elderfield, 2008; lines 10 and 13 in Figure 2) compared to the high temperature calibrations based on *Cibicidoides* spp. It has been shown that for temperature <3 °C, changes in Mg/Ca are for a large part caused by differences in carbonate ion saturation state ($\Delta[\text{CO}_3^{2-}]$), resulting in lower Mg/Ca (and hence lower temperatures) compared to “uncorrected” ratios (Elderfield et al., 2006). Therefore, one might argue that the Mg/Ca-BWT equations calibrated covering larger temperature ranges are more reliable and also more in line with the range of temperatures covered here.

In this study, foraminifera were not identified at species level, and it is likely that over the long time span studied here, different species were measured. As we are investigating long term and relatively large changes in Mg/Ca and hence temperature, small differences in calibrations within genera will have little impact on the reconstructed trends. Therefore, a Mg/Ca-BWT calibration based on different *Cibicidoides* spp. is used here to translate the obtained Mg/Ca to past BWTs. We applied both the calibration of Martin et al. (2002) and Lear et al. (2002). Lear et al. (2002) refined the calibration of Rosenthal et al. (1997) by the analysis of *C. wuellerstorfi*, *C. pachyderma*, *C. compressus*, and a *wuellerstorfi*-like *Cibicidoides*, from different ocean basins, and adding Mg/Ca data for BWTs lower than 4 °C. Similarly, Martin et al. (2002) extended the core top calibration of Rosenthal et al. (1997) to an even lower BWT (−1 °C). The two calibrations have the same temperature sensitivity ($B = 0.109$) but, due to different pre-exponential constants (A), differ 3.1 °C in absolute temperatures. Since our BWTs are likely >4 °C, and the paleodepth of the site remained well above the calcium carbonate compensation depth (CCD), we do not consider the potential effect of changes in carbonate ion concentration $\Delta(\text{CO}_3^{2-})$ on foraminiferal geochemistry.

The standard errors associated with the calibrations of Lear et al. (2002) and Martin et al. (2002) are 1.7 and 1.4 °C, respectively. There are no Mg/Ca-temperature calibrations developed for *Gavelinella* and *Lenticulina*. In the absence of appropriate calibrations of phylogenetically closely related species, we applied the *Cibicidoides* calibrations of Lear et al. (2002) and Martin et al. (2002). For *Epistomina*, we applied the Atlantic Mg/Ca-temperature of Rosenthal et al. (2006), but since *Epistomina* is a species producing aragonite, we also applied the Atlantic Sr/Ca-temperature calibration of Rosenthal et al. (2006), with a standard error of 1.1 °C.

2.4.2. Seawater Mg/Ca and Sr/Ca

The Mg/Ca ratio in the seawater has fluctuated on time scales of millions of years, which has been estimated in numerous models and using proxies over time (e.g., Coggon et al., 2010; Evans et al., 2018; Farkas et al., 2007; Lowenstein et al., 2001; Stanley & Hardie, 1998; Wilkinson & Algeo, 1989). We here apply the reconstruction of Farkas et al. (2007). This model overall agrees with older studies (e.g., Demicco et al., 2005; Stanley & Hardie, 1998), and with proxy data based on fluid inclusions (Horita et al., 2002; Lowenstein et al., 2001), but starts to deviate from the other models as well as from the data derived from echinoderms (Dickson, 2004) and mid-ocean ridge flank carbonate veins (Coggon et al., 2010) toward the Eocene and Paleocene. The recently published seawater Mg/Ca reconstruction based on coupled foraminiferal clumped isotope-Mg/Ca data of Evans et al. (2018) agrees mostly with the model of Stanley and Hardie (1998) for the Oligocene but approaches the model of Farkas et al. (2007) for the Eocene and Oligocene. Since the reconstruction of Evans et al. (2018) only spans the Eocene and first part of the Oligocene, we applied the model of Farkas et al. (2007). However, to illustrate the effect of the uncertainty in seawater Mg/Ca-values, we apply different seawater Mg/Ca values based on different model/proxy studies, for the age interval of 50 Ma, and calculated associated BWTs.

To reconstruct temperature from the Sr/Ca ratio in *Epistomina*, preserved in the sediments of ~91 Ma, we also have to assume a seawater Sr/Ca_{sw} ratio. We apply a value of ~11 mmol/mol as deduced from the Phanerozoic Sr/Ca_{sw} trend from Steuber and Veizer (2002), who reconstructed seawater Sr/Ca based on bivalve and belemnite analysis.

2.5. $\delta^{18}\text{O}$ and Δ_{47} Calibration

The temperature equation of Kim and O'Neil, J. R. (1997) was used to translate the benthic oxygen isotope data into paleo-BWTs. Bemis et al. (1998) suggested that *Cibicidoides* precipitates its shell close to predicted oxygen isotope equilibrium values and that *Cibicidoides* data derived from core tops from all over the world showed excellent agreement with the equation of Kim and O'Neil, J. R. (1997). Therefore, no correction

factor has been applied to the measured *Cibicidoides* $\delta^{18}\text{O}$ values. For *Epistomina* spp., the linear equation for *H. elegans* of Marchitto et al. (2014) was used. Wendler et al. (2013) observed a $\delta^{18}\text{O}$ offset of approximately 0.5‰ between *Lenticulina* species and *Berthelina berthelini* (morphologically closely resembling *Cibicidoides wuellerstorfi*) in a Turonian equatorial record from SE Tanzania. Applying the precise correction requires identification of the exact *Lenticulina* species, but as we have not distinguished between species within this genus, we apply the average correction of +0.5‰. As *Gavelinella* and *Cibicidoides* spp. overlap at the age interval of 78 Ma, we correct the *Gavelinella*-derived BWTs for the offset with the *Cibicidoides*-derived BWTs for this age. For ages of 50 Ma and older, ice-free conditions were assumed, with average global standard mean ocean water (SMOW) $\delta^{18}\text{O}$ being approximately -1‰ (Shackleton & Kennett, 1975). For the ages of ~33 and 41 Ma, $\delta^{18}\text{O}_{\text{SMOW}}$ values of -0.25‰ and -0.75‰ were assumed, respectively, based on the estimated variation in global average $\delta^{18}\text{O}_{\text{SMOW}}$ calculated by Lear et al. (2000). These values may not reflect all aspects of Earth's climate and (subtle) changes therein, as for instance there is evidence for Paleocene glaciation (Hollis et al., 2014), and local factors such as evaporation (Zachos et al., 1994) may affect the local seawater $\delta^{18}\text{O}$. We applied a -0.27‰ correction to translate SMOW to VPDB. For the planktonic foraminifera we also applied the equation of Kim and O'Neil, J. R. (1997) and assumed identical seawater $\delta^{18}\text{O}$ values as for the benthics. To translate Δ_{47} values to BWTs, we used the temperature calibration of Kele et al. (2015), based on inorganic calcite precipitation. We used the updated version of the Kele calibration ($\Delta_{47} = [0.04451 \pm 0.001004 \times 10^6]/T^2 + [0.171 \pm 0.01081]$; Bernasconi et al., 2018), after recalculating the calibration set with the Brand parameters (Daëron et al., 2016). This calibration is fully consistent with the recent calibration developed for planktonic and benthic foraminifera of Peral et al. (2018).

2.5.1. TEX_{86} and MAT_{mrs} Calibration

TEX_{86} values were calculated using the original ratio as defined by Schouten et al. (2002). For the translation to SSTs, there are multiple global core-top calibrations available (e.g., Kim et al., 2008; Liu et al., 2009; Schouten et al., 2002; Tierney & Tingley, 2014, 2015). Two logarithmic equations were proposed by Kim et al. (2010), that is, $\text{TEX}_{86}^{\text{L}}$ and $\text{TEX}_{86}^{\text{H}}$. The first mentioned is the logarithmic TEX_{86} without the crenarchaeol isomer and with GDGT-3 removed from the numerator, and it was shown to be suitable for subpolar Southern Ocean sediments. In contrast, the $\text{TEX}_{86}^{\text{H}}$ function, a logarithmic function of TEX_{86} , yields the best correlation with SST, when (sub)polar ocean data were removed. Additionally, core-top data from the Red Sea were removed from the $\text{TEX}_{86}^{\text{H}}$ calibration, since the TEX_{86} appeared to behave differently in this region compared to other oceanic regions due to distinctly different Thaumarchaeotal populations (Eder et al., 2002; Ionescu et al., 2009; Qian et al., 2011). More recently, Tierney and Tingley (2014, 2015) described a different approach using Bayesian statistics for the calibration of TEX_{86} , called BAYSPAR. The authors developed this calibration to address the differences in TEX_{86} response to temperature across different oceanic regions (Ho et al., 2014; Trommer et al., 2009), spatial trends in the residuals of other calibration models (Tierney, 2014; Tierney & Tingley, 2014), and the necessity for uncertainty propagation to derive estimates for uncertainties in reconstructed temperatures (Tierney & Tingley, 2014, 2015). We have applied both calibrations, and since the outcomes are similar for most intervals, we have solely plotted the $\text{TEX}_{86}^{\text{H}}$ -derived temperatures in Figures 3 and 4 and included BAYSPAR-derived temperatures in Figures 5 and S5a. The calibration error of $\text{TEX}_{86}^{\text{H}}$ is $\pm 2.5\text{ °C}$ (Kim et al., 2010). We also estimated subsurface temperatures using TEX_{86} , using both the BAYSPAR calibration and the calibration of Kim et al. (2012), as TEX_{86} is well known to contain a subsurface signal. For the BAYSPAR calibrations we assumed a prior temperature of 30 °C for SST and 20 °C for subsurface temperatures. We applied a prior standard deviation of 20 and a search tolerance of 0.2 (default settings).

To assess secondary effects potentially affecting the $\text{TEX}_{86}^{\text{H}}$ index, we applied four GDGT indices: (1) the branched isoprenoid tetraether (BIT) index, a proxy for soil organic matter input into the marine environment, as described by Hopmans et al. (2004); (2) the Methane Index, a proxy for dissociation of marine gas hydrates favoring anaerobic oxidation of methane, as proposed by Zhang et al. (2011); (3) %GDGT-0, a ratio reflecting sedimentary methanogenic archaeal GDGT production (Sinninghe Damsté et al., 2012), (4) and the Ring Index, which indicates nontemperature factors or nonmodern TEX_{86} -SST relations (Zhang et al., 2016). The MAT_{mrs} index is used as proxy for mean annual air temperature (MAT), based upon the distribution of branched GDGT (brGDGT) lipids (de Jonge et al., 2014). The MAT_{mrs} is a multiple linear regression based on the abundance of the major brGDGTs. We chose this calibration over the MAT_{mr} (de Jonge et al., 2014), as this latter calibration includes all 15 brGDGTs. Especially for the youngest age

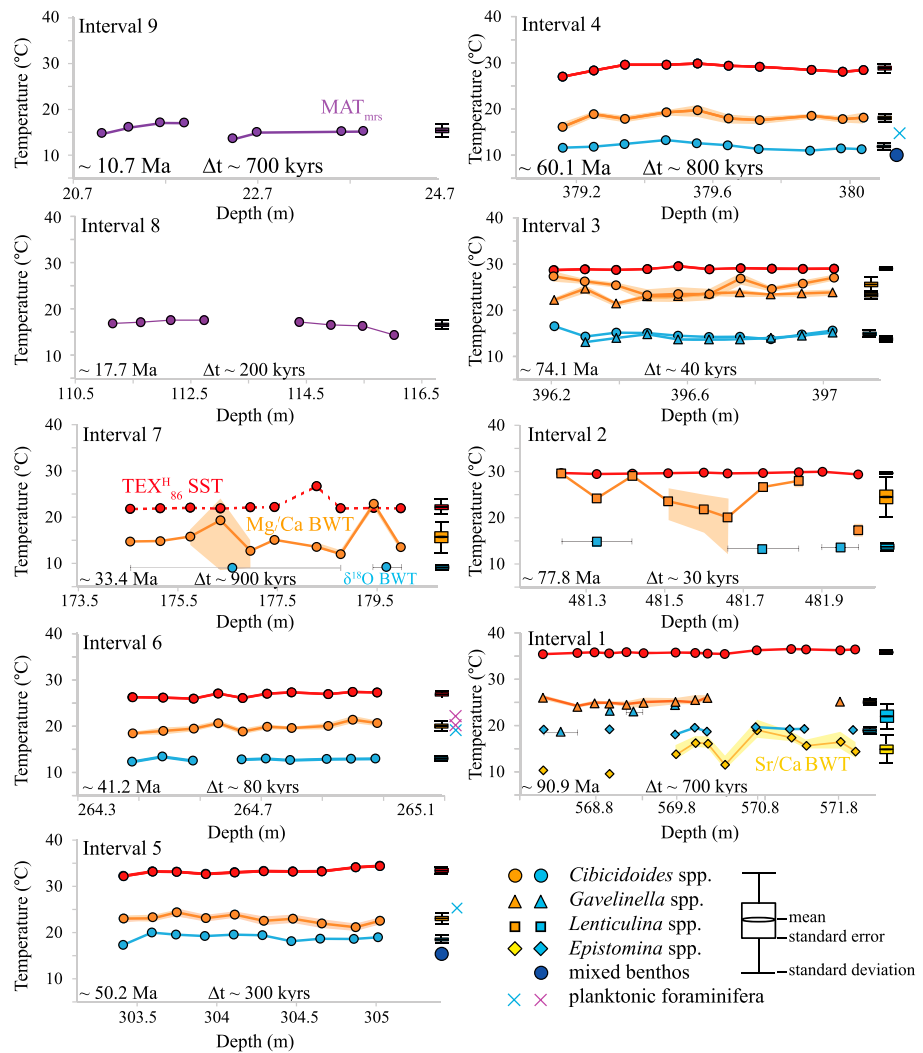


Figure 3. Short-term, temperature trends based on the different proxies. The timespans (in kyrs), abbreviated as Δt , are estimates only, since the age model is of low resolution (million-year scale). MAT_{mrs} is in purple; $\text{TEX}_{86}^{\text{H}}$ is in red; and Mg/Ca, Sr/Ca, and $\delta^{18}\text{O}$ are in orange, yellow, and blue, respectively. The $\text{TEX}_{86}^{\text{H}}$ temperatures for interval 7 are dashed, since these temperatures are likely affected by contribution of terrestrially derived GDGTs. For Mg/Ca we solely plotted the temperatures as calculated after Martin et al. (2002). The orange (or yellow) envelopes represent ± 1 Mg/Ca (or Sr/Ca) standard error (σ/\sqrt{n}) propagated into the temperature translation. Right from the temperature trends we plotted the mean, standard errors (σ/\sqrt{n}), and standard deviations ($\pm 1\sigma$ from mean), as well as the mean Δ_{47} -derived BWTs for the intervals of 50 and 60 Ma (dark blue dots), and planktonic $\delta^{18}\text{O}$ -derived temperatures for 41, 50, and 60 Ma (purple = *Acarinina* spp, blue = *Subbotina* and *Parasubbotina* spp.). For the time slice of 91 Ma, the Mg/Ca- and $\delta^{18}\text{O}$ -BWTs were corrected for the offset between *Cibicidoides* spp. and *Gavelinella* spp. at 74 Ma. MAT = mean annual air temperature; SST = sea surface temperature; BWT = bottom water temperature; GDGT = glyceryl dialkyl glyceryl tetraether.

interval, that is, 11 Ma, the brGDGT abundances are generally low, complicating the calculation of the MAT_{mrs} . The calibration error for the MAT is 5.0 °C (de Jonge et al., 2014).

3. Results

3.1. Foraminiferal Proxy Temperatures

Figure 3 shows the short-term temperature variability for all proxies, except for those based on clumped isotopes, as these were not analyzed on this temporal resolution. For the ages of approximately 18 and 11 Ma (intervals 8 and 9), there is no stable isotope, nor Mg/Ca data available due to the lack of (sufficient well-

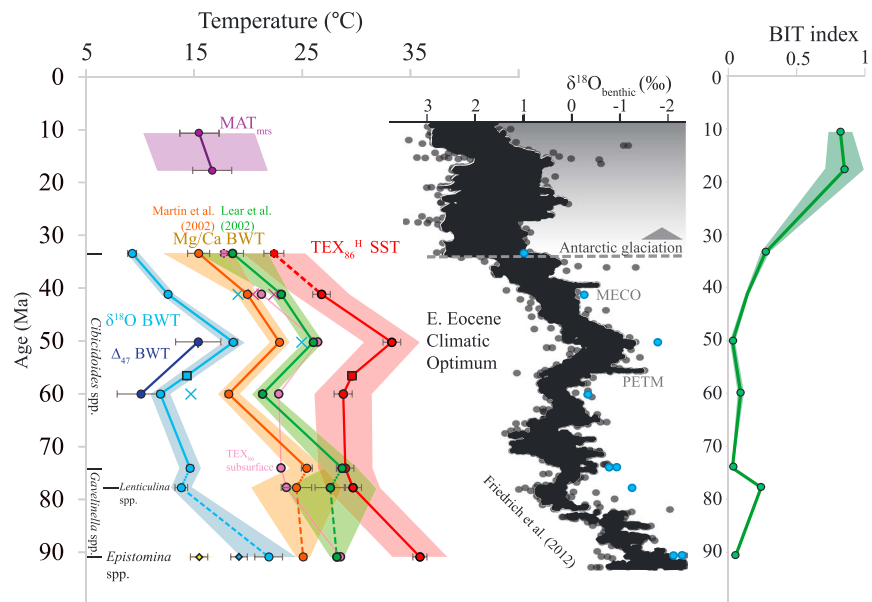


Figure 4. Proxy results for the Bass River core: clumped isotopes = dark blue dots; benthic $\delta^{18}\text{O}$ = light blue dots; benthic Mg/Ca = orange (Martin et al., 2002) and green (Lear et al., 2002) dots; TEX_{86} = red ($\text{TEX}_{86}^{\text{H}}$) and pink (subsurface) dots; MAT_{mrs} = purple dots; planktonic $\delta^{18}\text{O}$ = purple (*Acarinina* spp.) and blue (*Subbotina* and *Parasubbotina* spp.) crosses. Proxy values based on *Epistomina* spp. (aragonitic) are displayed as diamonds. The transparent envelopes represent the short term variation (standard deviations) within the age intervals (not plotted for subsurface TEX_{86}), and for benthic $\delta^{18}\text{O}$, TEX_{86} and MAT_{mrs} propagated with calibration errors of 0.13‰ (Rohling, 2007), 2.5 °C (Kim et al., 2010) and 5.0 °C (de Jonge et al., 2014), respectively. Temperature reconstructions not based on *Cibicidoides* spp. are dashed. The $\text{TEX}_{86}^{\text{H}}$ temperature for 33 Ma is dashed, since this temperature is likely affected by contribution of terrestrially derived GDGTs. Additionally, we plotted the pre-PETM $\delta^{18}\text{O}$ and $\text{TEX}_{86}^{\text{H}}$ temperatures (~56.5 Ma) for the Bass River site (John et al., 2008; Sluijs et al., 2007; diamond symbols). The error bars plotted for all proxies represent the standard errors. The middle panel shows the global benthic $\delta^{18}\text{O}$ compilation (modified after Friedrich et al., 2012), overlain by the $\delta^{18}\text{O}$ data of this study (blue dots). The right panel shows the BIT (dark green) indicated events: MECO = middle Eocene climatic optimum; EECO = early Eocene climate optimum; PETM = Paleocene Eocene thermal maximum; MAT = mean annual air temperature; SST = sea surface temperature; BWT = bottom water temperature; GDGT = glyceryl dialkyl glyceryl tetraether; BIT = branched isoprenoid tetraether.

preserved) foraminifera, related to the relatively shallow paleodepth of the core site at these times. The ranges in benthic $\delta^{18}\text{O}$ -derived temperatures within the high-resolution intervals are between 0.3 and 2.8 °C for the ages of 33 to 78 Ma (intervals 7 and 3). Only interval 1 (91 Ma) contains higher variability for the *Gavelinella* spp. $\delta^{18}\text{O}$ -derived temperatures with a range of 5.7 °C (Figure 3). In case of insufficient numbers of foraminifer specimens per sample for $\delta^{18}\text{O}$ analysis, samples were combined, reflected by the horizontal gray error bars in Figure 3.

The Mg/Ca values are also relatively constant for the ages of ~41, 50, 60, 74, and 91 Ma (intervals 6, 5, 7, 8, and 9, respectively), with a maximum variability of 4.1 °C. The reconstructed Mg/Ca-BWTs at 78 and 33 Ma show a larger range, that is, 12.3 and 10.9 °C, respectively. However, this is likely due to insufficient numbers of replicates measured, that is, less than 10 specimens for some subsamples, due to the scarcity of well-preserved foraminifera. For the intervals of 33 and 78 Ma, some measurements were based on one specimen only. At 78 Ma (interval 3), the observed large variation is mainly due to the high interspecimen variability in the Mg/Ca values measured on the *Lenticulina* spp. specimens.

For the *Epistomina* spp., the Mg/Ca value (after correction for the $\text{Mg}/\text{Ca}_{\text{sw}}$) falls outside the calibration range (using the Atlantic calibration for *H. elegans*; Rosenthal et al., 2006), and extrapolating the calibration results in unrealistically low temperatures (around -5 °C). Therefore, we applied the Sr/Ca-temperature calibration, as reported by Rosenthal et al. (2006), which is developed for foraminifera with aragonite shells. As mentioned in the method section, we applied a $\text{Sr}/\text{Ca}_{\text{sw}}$ value of ~11 mmol/mol after Steuber and Veizer (2002). This leads to a BWT of ~15.5 +/- 2.6 °C (yellow diamond, Figure 4). Coggon

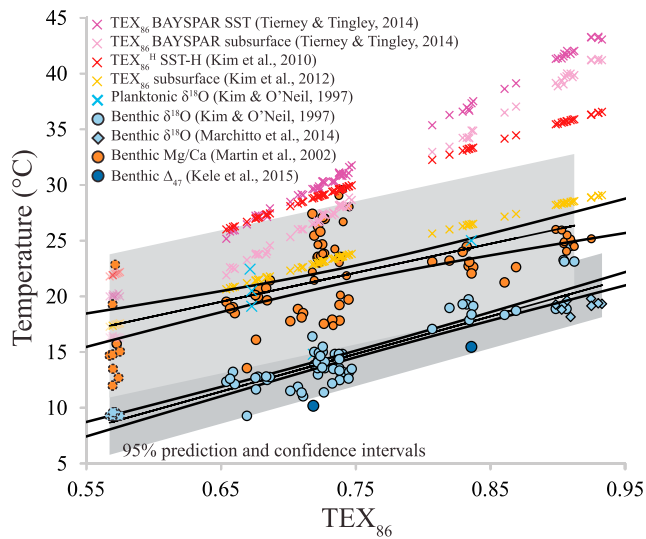


Figure 5. Cross-correlation between TEX_{86} values and benthic $\delta^{18}\text{O}$ (blue circles and diamonds), planktonic $\delta^{18}\text{O}$ (blue crosses), Mg/Ca (orange circles; calibration of Martin et al., 2002), and clumped isotope (dark blue circles) temperatures and temperatures of different TEX_{86} calibrations (Kim et al., 2010, 2012; red and yellow crosses; Tierney & Tingley, 2014, 2015; light and dark purple crosses). The lowest TEX_{86} values for 33 Ma are dashed (circle symbols for $\delta^{18}\text{O}$ and Mg/Ca vs. TEX_{86}) and transparent (crosses reflecting different TEX_{86} calibrations), since these values are likely affected by contribution of terrestrially derived GDGTs and therefore should be interpreted with caution. The two regression lines and corresponding prediction and confidence intervals are plotted for the correlations between TEX_{86} and $\delta^{18}\text{O}$ - and Mg/Ca-derived temperatures. SST = sea surface temperature.

et al. (2010) also estimated seawater Sr/Ca (based on calcium carbonate veins), but they suggest a value between 2 and 3 mmol/mol, which in combination with our results leads to unrealistic temperature estimates (around 155 °C).

Averaging the short-term Mg/Ca, Sr/Ca, and benthic $\delta^{18}\text{O}$ temperatures results in the long-term low-resolution temperature trend (Figure 4). Over the record, benthic foraminiferal $\delta^{18}\text{O}$ gradually increases over time, ranging from approximately -2.4‰ to 1.0‰ , corresponding with a cooling of around 12.6 °C (Figure 4). The isotopic offsets between the different benthic genera are relatively small (between *Cibicidoides* spp. and *Gavelinella* spp. at 74 Ma: 0.16‰ ; between *Gavelinella* spp. and *Epistomina* spp. at 91 Ma: 0.21‰). Around 50 Ma (interval 5), the oxygen isotope ratios reveal a negative excursion of around 1.5‰ . The clumped isotope (Δ_{47}) derived BWTs are 15.4 ± 2.1 °C and 10.1 ± 2.2 °C. The error indicates analytical uncertainty (1 standard error on the mean of 18 to 23 replicate analysis). The Mg/Ca values of the calcitic shells of *Cibicidoides*, *Gavelinella*, and *Lenticulina* spp. vary between approximately 3 and 14 mmol/mol over time, where Sr/Ca of the aragonitic *Epistomina* spp. reveals values of approximately 3 mmol/mol (~91 Ma; interval 1).

Overall, the Mg/Ca-based temperature gradient shows a similar cooling trend as the $\delta^{18}\text{O}$ -based BWT reconstruction, with exception of the reconstructed temperatures between 91 and 74 Ma, which are similar, whereas the $\delta^{18}\text{O}$ -BWTs decrease between 91 and 74 Ma (Figure 4). Also, the overall cooling from ~91 to 33 Ma inferred from Mg/Ca is smaller compared to that based on stable oxygen isotopes, that is, app. 9.7 °C versus 12.6 °C (not taking the *Epistomina* spp. temperatures into account), but this difference is probably not appreciable in view of the calibration and measurement

errors associated with the proxies. The overall long-term BWT variability as reconstructed by Mg/Ca and benthic $\delta^{18}\text{O}$ is in general larger (~10 to 13 °C) compared to the short-term variations (except for the Mg/Ca BWTs at 33 and 78 Ma; intervals 7 and 3), as well as the calibration errors: 1.4 and 1.7 °C for the Mg/Ca calibrations (Lear et al., 2002; Martin et al., 2002) and ~0.5 °C for $\delta^{18}\text{O}$ -BWT translation (Rohling, 2007).

The planktonic $\delta^{18}\text{O}$ -derived temperatures for age interval 6 (41 Ma) are 22.4 °C for *A. collectea*, 20.5 °C for *A. pseudotopilensis*, and 19.1 °C for *P. varianta*. For the age interval of 50 Ma (interval 5), the *Subbotina* spp.-derived temperature is 25.0 °C, and the average temperature for 60 Ma (interval 4) is 14.8 ± 0.5 °C based on *S. velascoensis*. The latter temperature is based on four measurements, whereas the other temperatures reflect one analysis only.

3.2. Organic Proxies

We were not able to calculate the $\text{U}^{K'}_{37}$ index, since no triunsaturated C_{37} (and C_{38}) long-chain ketones were detected; that is, the $\text{U}^{K'}_{37}$ index was always 1, something previously observed for sediments older than ~55 Ma (Brassell, 2014 and references cited therein). Diunsaturated alkenones were detected in the sediments of 33, 41, 50, 78, and 91 Ma (intervals 7, 6, 5, 3, and 1, respectively). Isoprenoid (for TEX_{86}) and branched GDGTs (for BIT and MAT_{mrs}) were always present above quantification limit, with exception of three sediments of the two youngest intervals 9 and 8 (11 and 18 Ma). The two youngest sediment intervals reveal high BIT indices of 0.82 and 0.85, respectively. Consequently, the MAT_{mrs} index, a proxy for air temperature, was determined for these age intervals. This revealed MATs of 15.5 and 16.7 °C for 11 and 18 Ma, respectively, revealing stable short-term trends (maximal variability of 3.5 °C, respectively; Figure 3). For all sediments older than 33 Ma, the BIT index was smaller than 0.34, suggesting that the $\text{TEX}_{86}^{\text{H}}$ was not substantially affected by soil organic matter input (Weijers et al., 2006), consistent with previous results for specific intervals at Bass River (Sluijs et al., 2007; van Helmond et al., 2014) or nearby sites (Vellekoop et al.,

2016), and hence, the $\text{TEX}_{86}^{\text{H}}$ was calculated to estimate seawater temperatures. To assess potential secondary influences on the TEX_{86} , we calculated the Methane Index, %GDGT-0, and Ring Index for these sediments. The highest values we obtained were 0.24, 43, and 0.3 (for ΔRI), respectively, which are all below the recommended threshold values of 0.3 to 0.5, 67, and 0.3, respectively (Sinninghe Damsté et al., 2012; Zhang et al., 2011, 2016), suggesting that the potential effects of confounding factors assessed with these indices are minor.

Between the samples from each depth interval, variability in the $\text{TEX}_{86}^{\text{H}}$ temperatures is between 0.5 and 4.9 °C, indicating that short-term variability is relatively modest (Figure 3) compared to the overall long-term trend observed in SST (22.4 to 35.9 °C) as well as the uncertainty related to the SST estimates (± 2.5 °C). Subsurface (0–200 m) temperatures, as calculated using the calibration of Kim, Romero, et al. (2012), range between 17.8 and 28.6 °C over the long-term record. Throughout the record, there is a clear cooling trend over time, with SST estimates decreasing from approximately 36 °C at 91 Ma to 22 °C at 33 Ma (Figure 4). Around 50 Ma there is an interruption in this trend, revealing SSTs of around 33 °C during the Early Eocene.

4. Discussion

4.1. Temperatures Based on Foraminiferal Calcite

Benthic foraminiferal $\delta^{18}\text{O}$ -based temperatures are calculated by assuming a past seawater stable oxygen isotope composition. As mentioned in the methods section, we assumed ice-free conditions for ages older than 50 Ma, associated with an average global $\delta^{18}\text{O}_{\text{SMOW}}$ of -1‰ (Shackleton & Kennett, 1975), and for the ages of ~33 and 41 Ma, $\delta^{18}\text{O}_{\text{SMOW}}$ values of -0.25‰ and -0.75‰ were assumed, respectively (Lear et al., 2000). However, seawater $\delta^{18}\text{O}$ can vary locally, and therefore, these values may not accurately reflect the seawater oxygen isotopic composition at Bass River. The reconstructed temperatures based on *Gavelinella* spp. (74 and 91 Ma) were corrected for the $\delta^{18}\text{O}$ -temperature difference between *Gavelinella* and *Cibicidoides* spp. at 74 Ma (i.e., normalized to *Cibicidoides* spp. temperatures). The resulting BWT at 91 Ma (*Gavelinella* spp.) is 21.9 °C, as compared to the BWT estimate of 19.2 °C based on *Epistomina* spp. for this time interval, using the temperature calibration of Marchitto et al. (2014). The oldest time interval (~91 Ma; ~570-m depth) is younger than the Cenomanian/Turonian boundary (~94 Ma; ~590-m depth; Sugarman et al., 1999). Similar to our study, Sugarman et al. (1999) analyzed stable oxygen isotopes on the *Gavelinella* spp. and *Epistomina* spp. specimens. They obtained $\delta^{18}\text{O}$ values around -3‰ and -2.5‰ for the two genera, respectively, across the Cenomanian/Turonian sequence, which is very similar to our average values of approximately -2.4‰ and -2.1‰ .

For calculating temperatures based on planktonic foraminiferal $\delta^{18}\text{O}$, we assumed the same seawater isotopic composition as we used for the benthics, and we applied the Kim and O'Neil calibration, which we also used for the benthic foraminiferal $\delta^{18}\text{O}$. Planktonic $\delta^{18}\text{O}$ reflects the foraminiferal habitat within the water column, either close to the sea surface or somewhat deeper within the water column. We analyzed *Acarinina* and *Subbotina* spp. specimens, with *Acarinina* spp. being considered a surface dweller and *Subbotina* spp. a thermocline dweller, which will therefore reflect somewhat deeper water temperatures (D'Hondt & Zachos, 1998). A particular caveat of planktonic $\delta^{18}\text{O}$ is potential impact of preservation/diagenetic alteration at the seafloor, which can result in biasing temperatures toward colder values (Pearson et al., 2001; Schrag et al., 1995).

In theory, the Mg/Ca and $\delta^{18}\text{O}$ derived BWTs should yield the same temperatures, as both proxies are measured on the exact same specimens, measuring the oxygen isotope composition after the Mg/Ca was determined using LA-ICP-MS. Differences in reconstructed temperatures may be caused by uncertainties in the necessary assumptions of isotopic composition and elemental composition of the seawater and/or vital effects associated with the different proxies. Diagenesis might as well compromise the Mg/Ca-derived temperature estimate (e.g., Hoogakker et al., 2009; Hover et al., 2001). Since diagenesis is a known source in off-setting element/Ca ratios in specimens from this age and from these environments, specimens were carefully selected, and ablation profiles were individually carefully examined for contamination and internal consistency of the Mg-signal within the shell walls. Ablation profiles displayed relatively constant Mg/Ca throughout the shell walls, suggesting that the original signal was well preserved (Figure S3). Similarly as

Table 1
Sensitivity of Mg/Ca-Derived BWTs to Seawater Mg/Ca and the Propagating Effect in Applying Different Mg/Ca-BWT Calibrations

Time (Ma)	Foraminiferal Mg/Ca (mmol/mol)	Seawater Mg/Ca (mol/mol)	Mg/Ca-BWT (°C) ^a	Mg/Ca-BWT (°C) ^b
50	7.43	1.6 ^c	30.5	27.4
		2.2 ^d	27.6	24.4
		2.6 ^e	26.0	22.9
		3.6 ^f	23.1	19.9
		5.2 ^g	19.7	16.6

Note. BWT = bottom water temperature. For all calculated Mg/Ca-derived BWTs, the uncertainty is ± 0.6 °C. The $\delta^{18}\text{O}$ -derived BWT for this time interval is 18.6 ± 1.0 °C. Clumped isotope estimates yield a BWT of 15.4 °C. Solely three Mg/Ca-derived BWT estimates in this table are close to this value (19.9, 19.7, and 16.6 °C; bold values in the table). These values derive from the combination with the two highest Mg/Ca_{sw} values.

^aMg/Ca bottom water temperature calculated based on the calibrations of Lear et al. (2002). ^bMg/Ca bottom water temperature calculated based on the calibrations of Martin et al. (2002). ^cSeawater Mg/Ca ratio from Stanley and Hardie (1998). ^dSeawater Mg/Ca ratio from Evans et al. (2018). ^eSeawater Mg/Ca ratio from Farkas et al. (2007). ^fSeawater Mg/Ca ratio from Wilkinson and Algeo (1989). ^g5.2 mol/mol is the present-day seawater Mg/Ca ratio.

for the benthic $\delta^{18}\text{O}$, we normalized the Mg/Ca-derived BWTs for *Gavelinella* spp. to that of *Cibicidoides* spp., correcting for the BWT difference at 74 Ma where the genera overlap.

Arguably, the most important source for the uncertainty in deriving deep-time seawater temperatures from foraminiferal Mg/Ca is the uncertainty in past seawater Mg/Ca. Sensitivity of Mg/Ca-derived temperatures to seawater Mg/Ca is illustrated in Table 1. Here we apply different modeled or reconstructed values for seawater Mg/Ca ratios for the age interval of ~50 Ma (1.6–3.6 mol/mol; Evans et al., 2018, Farkas et al., 2007; Stanley & Hardie, 1998; Wilkinson & Algeo, 1989), as well as the modern day ratio of 5.2 mol/mol. The calculated BWTs range between approximately 31 and 17 °C. The $\delta^{18}\text{O}$ -derived BWT for this time interval is 18.6 ± 1.0 °C, and the Δ_{47} -derived BWT is 15.4 ± 2.2 °C. Solely three Mg/Ca-derived BWTs (19.9, 19.7, and 16.6 °C, highlighted in Table 1) are similar (when considering calculated uncertainties) to this value, based on Mg/Ca_{sw} values of 3.6 and 5.2 mol/mol. This would suggest that the seawater Mg/Ca was >3.6 mol/mol. Other studies that have tried to constrain past Mg/Ca_{sw} values in the same way also suggest relatively high values (e.g., Billups & Schrag, 2003; Lear et al., 2002). In these studies, as well as our study, the relation between the incorporation of Mg into the foraminiferal shell and the Mg/Ca of the seawater is assumed to be linear. However, several studies show that the incorporation of Mg in

foraminiferal calcite as a function of seawater Mg/Ca is best described as a power function, which implies that a linear fit overestimates reconstructed seawater temperatures when seawater Mg/Ca is lower (see for a summary Evans & Muller, 2012, and references therein). Accordingly, when constraining Mg/Ca_{sw} values for the Cenozoic based on foraminiferal Mg/Ca and $\delta^{18}\text{O}$ -derived temperatures, it is expected that the estimated Mg/Ca_{sw} values will be too high (Evans & Muller, 2012). This therefore potentially explains the observation that our Mg/Ca-BWTs are higher than our benthic $\delta^{18}\text{O}$ -derived temperatures (Figures 3 and 4).

4.2. Temperatures Based on Organic Proxies

In general, TEX₈₆^H-based temperatures are considered to reflect upper water column temperatures, as the core-top calibration data sets show a strong correlation with satellite-derived annual mean SSTs (Kim et al., 2008, 2010; Schouten et al., 2002; Tierney & Tingley, 2014). However, it has been shown that the TEX₈₆^H proxy might regionally and temporally be affected by GDGTs derived from the subsurface, and it also correlates well with 0- to 200-m temperatures (Kim et al., 2015; Kim, Crosta, et al., 2012; Tierney & Tingley, 2014). Recently, Zhang and Liu (2018) examined the export depth of the TEX₈₆ signal by correlating the TEX₈₆ core-top data between 30°N and 30°S with SST and subsurface temperatures (0–200, 0–500, and 0–1,000 m), and comparing the obtained latitudinal gradient with the present-day meridional surface and subsurface temperature profiles. The authors observed the best correlation between TEX₈₆ and SST concluding that overall the TEX₈₆ reflects near-surface to shallow subsurface (<200 m) water temperatures. Accordingly, we believe it is useful to apply both a surface and subsurface calibration and compare the reconstructions with the other independent proxy data. The TEX₈₆ subsurface temperatures (as calculated after Kim, Romero, et al., 2012) are on average ~6 °C lower compared to the TEX₈₆^H-SSTs (Figure 4). Although we cannot use the U₃₇^{K'} for estimating SST, the absence of alkatrienones in sediments after ~55 Ma is an indication of SSTs exceeding 27 °C (e.g., Prahl & Wakeham, 1987; Volkman et al., 1995).

4.3. Consistency Between Proxy Reconstructions

As discussed above, a possible reason for the higher Mg/Ca-BWTs compared to the $\delta^{18}\text{O}$ -derived BWTs is the assumed linear relation between the foraminiferal Mg incorporation and the Mg/Ca of the seawater, which results in overestimation of temperatures when seawater Mg/Ca was lower than today (Evans & Muller, 2012). Additionally, support for the robustness of the $\delta^{18}\text{O}$ -derived BWTs comes from the clumped isotope based BWTs estimates at ~60 and 50 Ma (10.1 ± 2.2 and 15.4 ± 2.1 °C), which are close to the $\delta^{18}\text{O}$ -derived BWT estimates of 11.9 ± 0.9 and 18.6 ± 1.0 °C, respectively. Since Δ_{47} is independent of

seawater $\delta^{18}\text{O}$ composition, and thus solely reflects seawater temperature, the observed general agreement between Δ_{47} and $\delta^{18}\text{O}$ -derived BWTs implies that our assumed $\delta^{18}\text{O}_{\text{sw}}$ (-1‰ SMOW) was realistic. Remaining offsets could be explained by a slightly different $\delta^{18}\text{O}_{\text{sw}}$.

The $\text{TEX}_{86}^{\text{H}}$ -based SST estimates are on average 13 to 17 °C higher than reconstructed BWTs based on benthic foraminiferal $\delta^{18}\text{O}$, probably reflecting the different positions in the water column of the Thaumarchaeota and benthic foraminifera. This absolute temperature difference between $\delta^{18}\text{O}$ -derived BWTs and $\text{TEX}_{86}^{\text{H}}$ -based SST reflects the thermal gradient in the water column and is in line with a strong thermocline during spring and summer in present-day New Jersey Shelf waters (Castelao et al., 2010), as well as previous regional reconstructions for the Paleocene Eocene thermal maximum (PETM) interval (e.g., John et al., 2008; Zachos et al., 2006). The planktonic foraminiferal temperatures for the ages of 41, 50, and 60 Ma are in between the $\delta^{18}\text{O}$ -derived BWTs and $\text{TEX}_{86}^{\text{H}}$ SSTs. When assuming that $\text{TEX}_{86}^{\text{H}}$ reflects SST, the planktonic foraminiferal temperatures seem reasonable in view of the ecology of the species used here. *Acarinina* spp.-derived temperatures for 41 Ma are $\sim 4\text{--}6$ °C lower compared to the $\text{TEX}_{86}^{\text{H}}$ SSTs. The temperature difference between $\text{TEX}_{86}^{\text{H}}$ and *Acarinina* spp. found by Zachos et al. (2006) for Paleocene-Eocene sediments from Wilson Lake showed a similar offset, whereas the *Morozovella*-derived temperatures agreed very well in that study with the $\text{TEX}_{86}^{\text{H}}$ -derived temperatures, suggesting that *Acarinina* lived somewhat deeper in the water column on the New Jersey Shelf compared to *Morozovella*. For the intervals of 41, 50, and 60 Ma we also analyzed the $\delta^{18}\text{O}$ of *Subbotina* spp., which suggests considerably lower temperature compared to the $\text{TEX}_{86}^{\text{H}}$, that is, between 7 and 12 °C, which is consistent with the fact that *Subbotina* spp. is considered a thermocline-dweller living deeper in the water column (D'Hondt & Zachos, 1998). Furthermore, the high $\text{TEX}_{86}^{\text{H}}$ SST estimates agree with the fact that $U^{K'}_{37}$ suggest SST > 27 °C for the time interval of 41 and 50 Ma (intervals 6 and 5). However, this is not the case for the 33-Ma interval, where $\text{TEX}_{86}^{\text{H}}$ indicates an average SST of 22 °C. Likely, the $\text{TEX}_{86}^{\text{H}}$ -suggested temperatures are underestimated due to terrestrial organic carbon addition, as for 9 out of the 10 subsamples the BIT is between 0.24 and 0.34 with $\text{TEX}_{86}^{\text{H}}$ SSTs suggesting values between 21.9 and 22.2 °C. For one sediment sample where the BIT is 0.11, the $\text{TEX}_{86}^{\text{H}}$ -derived temperature suggests a warmer sea surface (26.7 °C). This strongly suggests that for this time-interval (7) the $\text{TEX}_{86}^{\text{H}}$ is affected by, relatively moderate, amounts of terrestrially derived isoprenoid GDGTs, resulting in underestimation of SST. We note that the $\text{TEX}_{86}^{\text{H}}$ -derived subsurface temperatures agree better with the planktonic foraminiferal temperatures calculated for 41, 50, and 60 Ma (Figure 4), suggesting that the planktonic $\delta^{18}\text{O}$ likely reflects a shallow subsurface signal. Although all specimens were checked carefully using light microscopy, it is not possible to exclude the possibility that recrystallization affected the planktonic foraminiferal shells at or beneath the seafloor, which would also result in $\delta^{18}\text{O}$ -derived temperatures being underestimated.

4.4. Reconstructed Bottom and Surface Water Temperatures

Overall all proxies measured here over the entire record show an excellent internal consistency (Figures 4 and 5). Although large offsets in absolute temperature are observed based on the calibrations used, the different proxies and calibrations show the same trends and sensitivity. Only the BAYSPAR calibrations show a somewhat different trend (Figure 5). The trend in reconstructed temperature based on the Mg/Ca of the *Cibicidoides* spp. shows good agreement with those of the $\delta^{18}\text{O}$ and $\text{TEX}_{86}^{\text{H}}$ proxies (Figures 4 and 5). However, reconstructed Mg/Ca-BWTs for the older part of the record remain relatively constant, whereas the benthic $\delta^{18}\text{O}$ and $\text{TEX}_{86}^{\text{H}}$ temperature records show a clear cooling trend from 91 to 74 Ma. However, it should be noted that for these oldest intervals, we applied *Cibicidoides*-specific Mg/Ca calibrations, whereas we analyzed other genera. Therefore, these data should be interpreted with caution. For the overall trend, the absolute BWTs derived from the two different Mg/Ca-BWT calibrations (Lear et al., 2002; Martin et al., 2002) fall between the $\delta^{18}\text{O}$ -derived BWT estimates and $\text{TEX}_{86}^{\text{H}}$ SSTs. As discussed in the previous paragraph, Mg/Ca BWTs are potentially overestimated, whereas benthic $\delta^{18}\text{O}$ -based temperatures are more likely to be correct, which is also supported by the close agreement with the temperatures based on clumped isotopes. However, even though absolute Mg/Ca-derived temperatures might be compromised in deep-time applications due to erroneous assumptions, our Mg/Ca-BWT record shows that the proxy fundamentals likely stayed intact on the timescale studied here, since the reconstructed BWT trend agrees well among the proxies.

We also observe a good correlation between the trends of $\text{TEX}_{86}^{\text{H}}$ and benthic $\delta^{18}\text{O}$ -derived temperatures through time ($R^2 = 0.86$; $n = 81$; two-tailed t -test p value $\ll 0.05$). Irrespective of the calibration used, TEX_{86} closely mimics the temperature trends based on the other proxies. Since they also align well with global benthic stable oxygen isotope compilations (e.g., Friedrich et al., 2012; Zachos et al., 2008) (Figure 4), our reconstructed trend in temperatures likely reflects a global pattern. As expected the BWTs we reconstruct at Bass River are higher than the deep sea benthic stacks (Figure 4), which represents the difference between our relatively warm shelf and the deep sea. We have also plotted the average pre-PETM (~ 56.5 Ma) $\text{TEX}_{86}^{\text{H}}$ temperature for the Bass River according to Sluijs et al. (2007) in Figure 4 (red squared symbol), that is, ~ 29.6 °C. Similarly, the pre-PETM average BWT based on the *Cibicides* spp. derived $\delta^{18}\text{O}$ value of -0.89 of John et al. (2008) for the Bass River was plotted (blue squared symbol). This value was translated to BWT using the calibration of Kim and O'Neil, J. R. (1997) and a $\delta^{18}\text{O}_{\text{sw}}$ of -1% , resulting in a BWT of ~ 14.3 °C. These two temperatures also align well with the overall records. We record an ~ 6 °C drop in SST as derived from $\text{TEX}_{86}^{\text{H}}$ from 33.3 °C at 50.2 Ma to 26.8 °C at 41.2 Ma. The magnitude of this cooling is consistent with the concomitant 4 °C cooling at the tropical site 959, although it might be on the high side considering the relatively limited amplification of cooling toward extratropical areas (Cramwinckel et al., 2018). Subsequently, $\text{TEX}_{86}^{\text{H}}$ records a cooling of more than 4 to 22.4 °C at 33 Ma, which is similar to the magnitude of tropical cooling during the same time interval (Cramwinckel et al., 2018).

Consistent results of planktonic $\delta^{18}\text{O}$ and Mg/Ca, benthic $\delta^{18}\text{O}$, and TEX_{86} paleothermometry have also been obtained from the PETM at Bass River, and several other sites along the New Jersey Shelf (Babila et al., 2016; Cramer et al., 1999; John et al., 2008; Makarova et al., 2017; Sluijs et al., 2007; Zachos et al., 2006). The difference between $\text{TEX}_{86}^{\text{H}}$ surface (Sluijs et al., 2007) and $\delta^{18}\text{O}$ BWTs (John et al., 2008) is in the order of 10 to 15 °C at Bass River and somewhat smaller at the shallower site Wilson Lake (Zachos et al., 2006), consistent with our results of the vertical temperature gradient based on these proxies. Moreover, Zachos et al. (2006) reported similar temperature differences between TEX_{86} SSTs and planktonic foraminiferal $\delta^{18}\text{O}$ temperatures based on *Acarinina* spp. (assuming $\delta^{18}\text{O}_{\text{sw}} = -1\%$) for Wilson Lake as obtained here, that is, between ~ 5 and 10 °C. It should be noted, however, that sea level rise (Harris et al., 2010; Sluijs et al., 2008) and hydrographic changes (Babila et al., 2016; Makarova et al., 2017; Sluijs & Brinkhuis, 2009; Zachos et al., 2006) might have affected these results across the PETM.

Overall, the trend in all temperature reconstructions align well, indicating a general cooling over the past 91 Ma. Despite the relatively coarse resolution, our reconstruction clearly reflects the warm interval during the Early Eocene (early Eocene climatic optimum) (Cramwinckel et al., 2018; Zachos et al., 2008). The benthic $\delta^{18}\text{O}$ record agrees well in both trend and magnitude with previously published stable oxygen isotope compilations of benthic foraminifera for the last 115 Ma (Friedrich et al., 2012), also indicating a progressive increase in $\delta^{18}\text{O}$ throughout the Cenozoic. Also, the MAT_{mrs} temperatures seem to agree with the benthic oxygen isotope compilation in terms of the global temperature cooling trend, even though they reflect continental air temperatures rather than seawater temperatures.

5. Conclusions

We have combined benthic foraminifer-based ($\delta^{18}\text{O}$, Δ_{47} , Mg/Ca and Sr/Ca) and organic proxies for sea surface ($\text{TEX}_{86}^{\text{H}}$) or continental (MAT_{mrs}) temperature in a multiproxy low-resolution study, to investigate interproxy consistency back to ~ 90 Ma, for the ODP Bass River site (NJ, USA). Relative changes in the temperature proxy data show good mutual agreement and are consistent with existing open ocean records, implying that global signals are dominating the record. The $\text{TEX}_{86}^{\text{H}}$ -based SST and shallow subsurface temperature estimates show trends in agreement with other proxies. The benthic $\delta^{18}\text{O}$ -derived temperatures are further supported by clumped isotope BWTs between ~ 60 and 50 Ma. Deep-time, Mg/Ca paleothermometry likely comprises the largest error due to the propagation of multiple uncertainties, such as choice of Mg/Ca-BWT calibration, secular variation of seawater Mg/Ca over time, and uncertainties in the relationship between seawater Mg/Ca and foraminiferal Mg partitioning. This final calibration uncertainty likely explains the fact that Mg/Ca consistently overestimated temperatures in the more distant past as observed in this study. Although all proxies suffer from uncertainty propagation when applied deep time, the offsets between the $\text{TEX}_{86}^{\text{H}}$ -derived SSTs and $\delta^{18}\text{O}$ -derived BWTs remained relatively similar from 33 to 91 Ma. In addition, BWT reconstructions based on Mg/Ca generally show similar long-term temperature variations as

those based on $\text{TEX}_{86}^{\text{H}}$ and $\delta^{18}\text{O}$. These results indicate that the fundamental mechanisms responsible for the proxy relations to temperature remained constant over time.

Acknowledgments

We thank Jort Ossebaar, Wim Boer, Piet van Gaever, Ellen Hopmans, Denise Dorhout, and Inge van Dijk for analytical support. Henko de Stijger, Geert-Jan Brummer, Bridget Wade, and Robert Speijer (KU Leuven) are thanked for their help on foraminifer taxonomy and James Browning (Rutgers University, NJ) for core sampling. This work was carried out under the program of the Netherlands Earth System Science Centre (NESSC), financially supported by the Dutch ministry for Education, Culture and Science (OCW) (Grant 024.002.001). The supporting information is available at PANGAEA (<https://doi.pangaea.de/10.1594/PANGAEA.892907>).

References

- Anagnostou, E., John, E. H., Edgar, K. M., Foster, G. L., Ridgwell, A., Inglis, G. N., et al. (2016). Changing atmospheric CO_2 concentration was the primary driver of early Cenozoic climate. *Nature*, 533, 380. <https://doi.org/10.1038/nature17423>
- Andrews, G. W. (1988). *A revised marine diatom zonation for Miocene strata of the Southeastern United States*. U.S. Geological Survey Professional Paper, 1481, 29 p., 8 pls. Washington: United States Government Printing Office.
- Babila, T. L., Rosenthal, Y., Wright, J. D., & Miller, K. G. (2016). A continental shelf perspective of ocean acidification and temperature evolution during the Paleocene-Eocene thermal maximum. *Geology*, 44(4), 275–278. <https://doi.org/10.1130/g37522.1>
- Bemis, B. E., Spero, H. J., Bijma, J., & Lea, D. W. (1998). Reevaluation of the oxygen isotopic composition of planktonic foraminifera: Experimental results and revised paleotemperature equations. *Paleoceanography*, 13(2), 150–160. <https://doi.org/10.1029/98PA00070>
- Bernasconi, S. M., Müller, I. A., Bergmann, K. D., Breitenbach, S. F. M., Fernandez, A., Hodell, D. A., et al. (2018). Reducing uncertainties in carbonate clumped isotope analysis through consistent carbonate-based standardization. *Geochemistry, Geophysics, Geosystems*, 19, 2895–2914. <https://doi.org/10.1029/2017GC007385>
- Berner, R. A. (2004). A model for calcium, magnesium and sulfate in seawater over Phanerozoic time. *American Journal of Science*, 304(5), 438–453. <https://doi.org/10.2475/ajs.304.5.438>
- Bijl, P. K., Schouten, S., Sluijs, A., Reichert, G.-J., Zachos, J. C., & Brinkhuis, H. (2009). Early Palaeogene temperature evolution of the Southwest Pacific Ocean. *Nature*, 461(7265), 776–779. <https://doi.org/10.1038/nature08399>
- Billups, K., & Schrag, D. P. (2002). Paleotemperatures and ice volume of the past 27 Myr revisited with paired Mg/Ca and $\delta^{18}\text{O}$ measurements on benthic foraminifera. *Paleoceanography*, 17(1), 1003. <https://doi.org/10.1029/2000PA000567>
- Billups, K., & Schrag, D. P. (2003). Application of benthic foraminiferal Mg/Ca ratios to questions of Cenozoic climate change. *Earth and Planetary Science Letters*, 209(1–2), 181–195. [https://doi.org/10.1016/s0012-821x\(03\)00067-0](https://doi.org/10.1016/s0012-821x(03)00067-0)
- Blow, W. H. (1969). Late middle Eocene to recent planktonic foraminiferal biostratigraphy, biochronology and paleoclimatology. In P. Brönnimann, & H. H. Renz (Eds.), *Proceedings of the first international conference on planktonic microfossils*, (Vol. 1, pp. 199–422). Geneva, 1967: E. J. Brill, Leiden.
- Bowman, A. R., & Bralower, T. J. (2005). Paleoceanographic significance of high-resolution carbon isotope records across the Cenomanian-Turonian boundary in the Western interior and New Jersey coastal plain, USA. *Marine Geology*, 217(3–4), 305–321. <https://doi.org/10.1016/j.margeo.2005.02.010>
- Brassell, S. C. (2014). Climatic influences on the Paleogene evolution of alkenones. *Paleoceanography*, 29, 255–272. <https://doi.org/10.1002/2013pa002576>
- Brassell, S. C., Eglinton, G., Marlowe, I. T., Pflaumann, U., & Sarnthein, M. (1986). Molecular stratigraphy—A new tool for climatic assessment. *Nature*, 320(6058), 129–133. <https://doi.org/10.1038/320129a0>
- Burgess, C. E., Pearson, P. N., Lear, C. H., Morgans, H. E. G., Handley, L., Pancost, R. D., & Schouten, S. (2008). Middle Eocene climate cyclicity in the southern Pacific: Implications for global ice volume. *Geology*, 36(8), 651–654. <https://doi.org/10.1130/g24762a.1>
- Castelao, R., Glenn, S., & Schofield, O. (2010). Temperature, salinity, and density variability in the central Middle Atlantic Bight. *Journal of Geophysical Research*, 115, C02027. <https://doi.org/10.1029/2009JC006082>
- Chen, W., Mohtadi, M., Schefuß, E., & Mollenhauer, G. (2014). Organic-geochemical proxies of sea surface temperature in surface sediments of the tropical eastern Indian Ocean. *Deep-Sea Research Part I-Oceanographic Research Papers*, 88, 17–29. <https://doi.org/10.1016/j.dsr.2014.03.005>
- Coggon, R. M., Teagle, D. A. H., Smith-Duque, C. E., Alt, J. C., & Cooper, M. J. (2010). Reconstructing past seawater Mg/Ca and Sr/Ca from mid-ocean ridge flank calcium carbonate veins. *Science*, 327(5969), 1114–1117. <https://doi.org/10.1126/science.1182252>
- Conte, M. H., Sicre, M. A., Ruhlmann, C., Weber, J. C., Schulte, S., Schulz-Bull, D., & Blanz, T. (2006). Global temperature calibration of the alkenone unsaturation index (U^{K}_{37}) in surface waters and comparison with surface sediments. *Geochemistry Geophysics Geosystems*, 7, Q02005. <https://doi.org/10.1029/2005GC001054>
- Cramer, B. S., Aubry, M. P., Miller, K. G., Olsson, R. K., Wright, J. D., & Kent, D. V. (1999). An exceptional chronologic, isotopic, and clay mineralogical record of the latest Paleocene thermal maximum, Bass River, NJ, ODP 174AX. *Bulletin de la Societe Geologique de France*, 170(6), 883–897. <https://doi.org/10.7916/D8222RZR>
- Cramwinckel, M. J., Huber, M., Kocken, I. J., Agnini, C., Bijl, P. K., Bohaty, S. M., et al. (2018). Synchronous tropical and polar temperature evolution in the Eocene. *Nature*, 559(7714), 382–386. <https://doi.org/10.1038/s41586-018-0272-2>
- Daëron, M., Blamart, D., Peral, M., & Affek, H. P. (2016). Absolute isotopic abundance ratios and the accuracy of $\Delta 47$ measurements. *Chemical Geology*, 442, 83–96. <https://doi.org/10.1016/j.chemgeo.2016.08.014>
- Delaney, M. L., Be, A. W. H., & Boyle, E. A. (1985). Li, Sr, Mg, and Na in foraminiferal calcite shells from laboratory culture, sediment traps, and sediment cores. *Geochimica et Cosmochimica Acta*, 49(6), 1327–1341. [https://doi.org/10.1016/0016-7037\(85\)90284-4](https://doi.org/10.1016/0016-7037(85)90284-4)
- Demicco, R. V., Lowenstein, T. K., Hardie, L. A., & Spencer, R. J. (2005). Model of seawater composition for the Phanerozoic. *Geology*, 33(11), 877–880. <https://doi.org/10.1130/g21945.1>
- D'Hondt, S., & Zachos, J. C. (1998). Cretaceous foraminifera and the evolutionary history of planktic photosymbiosis. *Paleobiology*, 24(04), 512–523. <https://doi.org/10.1017/S0094837300020133>
- Dickson, J. A. D. (2004). Echinoderm skeletal preservation: Calcite-aragonite seas and the Mg/Ca ratio of Phanerozoic oceans. *Journal of Sedimentary Research*, 74(3), 355–365. <https://doi.org/10.1306/112203740355>
- Dissard, D., Nehrke, G., Reichert, G.-J., & Bijma, J. (2010). Impact of seawater pCO_2 on calcification and Mg/Ca and Sr/Ca ratios in benthic foraminifera calcite: Results from culturing experiments with *Ammonia tepida*. *Biogeosciences*, 7(1), 81–93. <https://doi.org/10.5194/bg-7-81-2010>
- Dueñas-Bohórquez, A., da Rocha, R. E., Kuroyanagi, A., Bijma, J., & Reichert, G.-J. (2009). Effect of salinity and seawater calcite saturation state on Mg and Sr incorporation in cultured planktonic foraminifera. *Marine Micropaleontology*, 73(3–4), 178–189. <https://doi.org/10.1016/j.marmicro.2009.09.002>
- Dueñas-Bohórquez, A., Raitzsch, M., de Nooijer, L. J., & Reichert, G.-J. (2011). Independent impacts of calcium and carbonate ion concentration on Mg and Sr incorporation in cultured benthic foraminifera. *Marine Micropaleontology*, 81(3–4), 122–130. <https://doi.org/10.1016/j.marmicro.2011.08.002>

- Eder, W., Schmidt, M., Koch, M., Garbe-Schönberg, D., & Huber, R. (2002). Prokaryotic phylogenetic diversity and corresponding geochemical data of the brine-seawater interface of the Shaban Deep, Red Sea. *Environmental Microbiology*, 4(11), 758–763. <https://doi.org/10.1046/j.1462-2920.2002.00351.x>
- Eiler, J. M. (2007). “Clumped-isotope” geochemistry—The study of naturally-occurring, multiply-substituted isotopologues. *Earth and Planetary Science Letters*, 262(3–4), 309–327. <https://doi.org/10.1016/j.epsl.2007.08.020>
- Elderfield, H., Cooper, M., & Ganssen, G. (2000). Sr/Ca in multiple species of planktonic foraminifera: Implications for reconstructions of seawater Sr/Ca. *Geochemistry, Geophysics, Geosystems*, 1(11), 1017. <https://doi.org/10.1029/1999GC000031>
- Elderfield, H., Vautravers, M., & Cooper, M. (2002). The relationship between shell size and Mg/Ca, Sr/Ca, $\delta^{18}\text{O}$, and $\delta^{13}\text{C}$ of species of planktonic foraminifera. *Geochemistry Geophysics Geosystems*, 3(8), 1052. <https://doi.org/10.1029/2001GC000194>
- Elderfield, H., Yu, J., Anand, P., Kiefer, T., & Nyland, B. (2006). Calibrations for benthic foraminiferal Mg/Ca paleothermometry and the carbonate ion hypothesis. *Earth and Planetary Science Letters*, 250(3–4), 633–649. <https://doi.org/10.1016/j.epsl.2006.07.041>
- Eldrett, J. S., Ma, C., Bergman, S. C., Lutz, B., Gregory, F. J., Dodsworth, P., et al. (2015). An astronomically calibrated stratigraphy of the Cenomanian, Turonian and earliest Coniacian from the Cretaceous Western Interior Seaway, USA: Implications for global chronostratigraphy. *Cretaceous Research*, 56, 316–344. <https://doi.org/10.1016/j.cretres.2015.04.010>
- Elling, F. J., Könneke, M., Lipp, J. S., Becker, K. W., Gagen, E. J., & Hinrichs, K.-U. (2014). Effects of growth phase on the membrane lipid composition of the thaumarchaeon *Nitrosopumilus maritimus* and their implications for archaeal lipid distributions in the marine environment. *Geochimica et Cosmochimica Acta*, 141, 579–597. <https://doi.org/10.1016/j.gca.2014.07.005>
- Elling, F. J., Könneke, M., Mussmann, M., Greve, A., & Hinrichs, K.-U. (2015). Influence of temperature, pH, and salinity on membrane lipid composition and TEX₈₆ of marine planktonic thaumarchaeal isolates. *Geochimica et Cosmochimica Acta*, 171, 238–255. <https://doi.org/10.1016/j.gca.2015.09.004>
- Evans, D., & Muller, W. (2012). Deep time foraminifera Mg/Ca paleothermometry: Nonlinear correction for secular change in seawater Mg/Ca. *Paleoceanography*, 27, PA4205. <https://doi.org/10.1029/2012PA002315>
- Evans, D., Sagoo, N., Renema, W., Cotton, L. J., Müller, W., Todd, J. A., et al. (2018). Eocene greenhouse climate revealed by coupled clumped isotope-Mg/Ca thermometry. *Proceedings of the National Academy of Sciences*. <https://doi.org/10.1073/pnas.1714744115>
- Farkas, J., Bohm, F., Wallmann, K., Blenkinsop, J., Eisenhauer, A., van Geldern, R., et al. (2007). Calcium isotope record of Phanerozoic oceans: Implications for chemical evolution of seawater and its causative mechanisms. *Geochimica et Cosmochimica Acta*, 71(21), 5117–5134. <https://doi.org/10.1016/j.gca.2007.09.004>
- Fernandez, A., Müller, I. A., Rodríguez-Sanz, L., van Dijk, J., Looser, N., & Bernasconi, S. M. (2017). A reassessment of the precision of carbonate clumped isotope measurements: Implications for calibrations and paleoclimate reconstructions. *Geochemistry, Geophysics, Geosystems*, 18, 4375–4386. <https://doi.org/10.1002/2017gc007106>
- Forster, A., Schouten, S., Moriya, K., Wilson, P. A., & Sinninghe Damsté, J. S. (2007). Tropical warming and intermittent cooling during the Cenomanian/Turonian oceanic anoxic event 2: Sea surface temperature records from the equatorial Atlantic. *Paleoceanography*, 22, PA1219. <https://doi.org/10.1029/2006pa001349>
- Foster, G. L., Royer, D. L., & Lunt, D. J. (2017). Future climate forcing potentially without precedent in the last 420 million years. *Nature Communications*, 8. <https://doi.org/10.1038/ncomms14845>
- Friedrich, O., Norris, R. D., & Erbacher, J. (2012). Evolution of middle to Late Cretaceous oceans—A 55 m.y. record of Earth's temperature and carbon cycle. *Geology*, 40(2), 107–110. <https://doi.org/10.1130/g32701.1>
- Frieling, J., Gebhardt, H., Huber, M., Adekeye, O. A., Akande, S. O., Reichart, G.-J., et al. (2017). Extreme warmth and heat-stressed plankton in the tropics during the Paleocene-Eocene thermal maximum. *Science Advances*, 3(3). <https://doi.org/10.1126/sciadv.1600891>
- Gradstein, F. M., Agterberg, F. P., Ogg, J. G., Hardenbol, J., Van Veen, P., Thierry, J., & Huang, Z. (1995). A Triassic, Jurassic and Cretaceous time scale. In W. A. Berggren, D. V. Kent, M. P. Aubry, & J. G. Hardenbol (Eds.), *Geochronology, time scales and global stratigraphic correlation*, (Vol. 54, pp. 95–126). SEPM Spec. Publ.
- Gradstein, F. M., Ogg, J. G., Schmitz, M. D., & Ogg, G. M. (2012). *The geologic time scale 2012*, (p. 1144). Oxford (UK): Elsevier.
- Harris, A. D., Miller, K. G., Browning, J. V., Sugarman, P. J., Olsson, R. K., Cramer, B. S., & Wright, J. D. (2010). Integrated stratigraphic studies of Paleocene-lowermost Eocene sequences, New Jersey Coastal Plain: Evidence for glacioeustatic control. *Paleoceanography*, 25, PA3211. <https://doi.org/10.1029/2009PA001800>
- Healey, S. L., Thunell, R. C., & Corliss, B. H. (2008). The Mg/Ca-temperature relationship of benthic foraminiferal calcite: New core-top calibrations in the <4 °C temperature range. *Earth and Planetary Science Letters*, 272(3–4), 523–530. <https://doi.org/10.1016/j.epsl.2008.05.023>
- Hernandez, J. C. M. K.G., Feigenson, M. (2000). ⁸⁷Sr/⁸⁶Sr dating of Upper Cretaceous (Campanian and Santonian) depositional sequences: Bass River and Ancora, NJ ODP Leg 174 AX. *The Rutgers Scholar*. doi available from World Wide Web: <http://rutgersscholar.rutgers.edu/volume02/millhern/millhern.htm>
- Ho, S. L., Mollenhauer, G., Fietz, S., Martinez-Garcia, A., Lamy, F., Rueda, G., et al. (2014). Appraisal of TEX₈₆ and TEX₈₆^L thermometries in subpolar and polar regions. *Geochimica et Cosmochimica Acta*, 131, 213–226. <https://doi.org/10.1016/j.gca.2014.01.001>
- Hollis, C. J., Tayler, M. J. S., Andrew, B., Taylor, K. W., Lurcock, P., Bijl, P. K., et al. (2014). Organic-rich sedimentation in the South Pacific Ocean associated with Late Paleocene climatic cooling. *Earth-Science Reviews*, 134, 81–97. <https://doi.org/10.1016/j.earscirev.2014.03.006>
- Hollis, C. J., Taylor, K. W. R., Handley, L., Pancost, R. D., Huber, M., Creech, J. B., et al. (2012). Early Paleogene temperature history of the Southwest Pacific Ocean: Reconciling proxies and models. *Earth and Planetary Science Letters*, 349–350, 53–66. <https://doi.org/10.1016/j.epsl.2012.06.024>
- Hoogakker, B. A. A., Klinkhammer, G. P., Elderfield, H., Rohling, E. J., & Hayward, C. (2009). Mg/Ca paleothermometry in high salinity environments. *Earth and Planetary Science Letters*, 284(3–4), 583–589. <https://doi.org/10.1016/j.epsl.2009.05.027>
- Hopmans, E. C., Weijers, J. W. H., Schefuss, E., Herfort, L., Sinninghe Damsté, J. S., & Schouten, S. (2004). A novel proxy for terrestrial organic matter in sediments based on branched and isoprenoid tetraether lipids. *Earth and Planetary Science Letters*, 224(1–2), 107–116. <https://doi.org/10.1016/j.epsl.2004.05.012>
- Horita, J., Zimmermann, H., & Holland, H. D. (2002). Chemical evolution of seawater during the Phanerozoic. *Geochimica et Cosmochimica Acta*, 66(21), 3733–3756. [https://doi.org/10.1016/s0016-7037\(01\)00884-5](https://doi.org/10.1016/s0016-7037(01)00884-5)
- Hover, V. C., Walter, L. M., & Peacor, D. R. (2001). Early marine diagenesis of biogenic aragonite and Mg-calcite: New constraints from high-resolution STEM and AEM analyses of modern platform carbonates. *Chemical Geology*, 175(3–4), 221–248. [https://doi.org/10.1016/s0009-2541\(00\)00326-0](https://doi.org/10.1016/s0009-2541(00)00326-0)

- Huguet, C., Schimmelmann, A., Thunell, R., Lourens, L. J., Sinninghe Damsté, J. S., & Schouten, S. (2007). A study of the TEX₈₆ paleothermometer in the water column and sediments of the Santa Barbara Basin, California. *Paleoceanography*, *22*, PA3003. <https://doi.org/10.1029/2006pa001310>
- Hurley, S. J., Elling, F. J., Konneke, M., Buchwald, C., Wankel, S. D., Santoro, A. E., et al. (2016). Influence of ammonia oxidation rate on thaumarchaeal lipid composition and the TEX₈₆ temperature proxy. *Proceedings of the National Academy of Sciences of the United States of America*, *113*(28), 7762–7767. <https://doi.org/10.1073/pnas.1518534113>
- Ionescu, D., Penno, S., Haimovich, M., Rihtman, B., Goodwin, A., Schwartz, D., et al. (2009). Archaea in the Gulf of Aqaba. *FEMS Microbiology Ecology*, *69*(3), 425–438. <https://doi.org/10.1111/j.1574-6941.2009.00721.x>
- John, C. M., Bohaty, S. M., Zachos, J. C., Sluijs, A., Gibbs, S., Brinkhuis, H., & Bralower, T. J. (2008). North American continental margin records of the Paleocene-Eocene thermal maximum: Implications for global carbon and hydrological cycling. *Paleoceanography*, *23*, PA2217. <https://doi.org/10.1029/2007PA001465>
- de Jonge, C., Hopmans, E. C., Zell, C. I., Kim, J. H., Schouten, S., & Sinninghe Damsté, J. S. (2014). Occurrence and abundance of 6-methyl branched glycerol dialkyl glycerol tetraethers in soils: Implications for palaeoclimate reconstruction. *Geochimica et Cosmochimica Acta*, *141*, 97–112. <https://doi.org/10.1016/j.gca.2014.06.013>
- Kele, S., Breitenbach, S. F. M., Capezzuoli, E., Meckler, A. N., Ziegler, M., Millan, I. M., et al. (2015). Temperature dependence of oxygen- and clumped isotope fractionation in carbonates: A study of travertines and tufas in the 6–95 °C temperature range. *Geochimica et Cosmochimica Acta*, *168*, 172–192. <https://doi.org/10.1016/j.gca.2015.06.032>
- Keul, N., Langer, G., Thoms, S., de Nooijer, L. J., Reichart, G.-J., & Bijma, J. (2017). Exploring foraminiferal Sr/Ca as a new carbonate system proxy. *Geochimica et Cosmochimica Acta*, *202*, 374–386. <https://doi.org/10.1016/j.gca.2016.11.022>
- Kim, J. H., Crosta, X., Willmott, V., Renssen, H., Bonnin, J., Helmke, P., et al. (2012). Holocene subsurface temperature variability in the eastern Antarctic continental margin. *Geophysical Research Letters*, *39*, L06705. <https://doi.org/10.1029/2012GL051157>
- Kim, J.-H., Romero, O. E., Lohmann, G., Donner, B., Laepple, T., Haam, E., & Sinninghe Damsté, J. S. (2012). Pronounced subsurface cooling of North Atlantic waters off Northwest Africa during Dansgaard-Oeschger interstadials. *Earth and Planetary Science Letters*, *339*–*340*, 95–102. <https://doi.org/10.1016/j.epsl.2012.05.018>
- Kim, J.-H., Schouten, S., Hopmans, E. C., Donner, B., & Sinninghe Damsté, J. S. (2008). Global sediment core-top calibration of the TEX₈₆ paleothermometer in the ocean. *Geochimica et Cosmochimica Acta*, *72*(4), 1154–1173. <https://doi.org/10.1016/i.gca.2007.12.010>
- Kim, J.-H., Schouten, S., Rodrigo-Gámiz, M., Rampen, S., Marino, G., Huguet, C., et al. (2015). Influence of deep-water derived isoprenoid tetraether lipids on the TEX₈₆ paleothermometer in the Mediterranean Sea. *Geochimica et Cosmochimica Acta*, *150*, 125–141. <https://doi.org/10.1016/j.gca.2014.11.017>
- Kim, J. H., van der Meer, J., Schouten, S., Helmke, P., Willmott, V., Sangiorgi, F., et al. (2010). New indices and calibrations derived from the distribution of crenarchaeal isoprenoid tetraether lipids: Implications for past sea surface temperature reconstructions. *Geochimica et Cosmochimica Acta*, *74*(16). <https://doi.org/10.1016/j.gca.2010.05.027>
- Kim, S. T., & O'Neil, J. R. (1997). Equilibrium and nonequilibrium oxygen isotope effects in synthetic carbonates. *Geochimica et Cosmochimica Acta*, *61*(16), 3461–3475. [https://doi.org/10.1016/s0016-7037\(97\)00169-5](https://doi.org/10.1016/s0016-7037(97)00169-5)
- Kisakirek, B., Eisenhauer, A., Bohm, F., Garbe-Schonberg, D., & Erez, J. (2008). Controls on shell Mg/Ca and Sr/Ca in cultured planktonic foraminifera, *Globigerinoides ruber* (white). *Earth and Planetary Science Letters*, *273*(3–4), 260–269. <https://doi.org/10.1016/j.epsl.2008.06.026>
- Lea, D. W., Mashiotta, T. A., & Spero, H. J. (1999). Controls on magnesium and strontium uptake in planktonic foraminifera determined by live culturing. *Geochimica et Cosmochimica Acta*, *63*(16), 2369–2379. [https://doi.org/10.1016/s0016-7037\(99\)00197-0](https://doi.org/10.1016/s0016-7037(99)00197-0)
- Lear, C. H., Elderfield, H., & Wilson, P. A. (2000). Cenozoic deep-sea temperatures and global ice volumes from Mg/Ca in benthic foraminiferal calcite. *Science*, *287*(5451), 269–272. <https://doi.org/10.1126/science.287.5451.269>
- Lear, C. H., Rosenthal, Y., & Slowey, N. (2002). Benthic foraminiferal Mg/Ca-paleothermometry: A revised core-top calibration. *Geochimica et Cosmochimica Acta*, *66*(19), 3375–3387. [https://doi.org/10.1016/s0016-7037\(02\)00941-9](https://doi.org/10.1016/s0016-7037(02)00941-9)
- Liu, X. L., Zhu, C., Wakeham, S. G., & Hinrichs, K. U. (2014). In situ production of branched glycerol dialkyl glycerol tetraethers in anoxic marine water columns. *Marine Chemistry*, *166*, 1–8. <https://doi.org/10.1016/j.marchem.2014.08.008>
- Liu, Z., Pagani, M., Zinniker, D., DeConto, R., Huber, M., Brinkhuis, H., et al. (2009). Global cooling during the Eocene-Oligocene climate transition. *Science*, *323*(5918), 1187–1190. <https://doi.org/10.1126/science.1166368>
- Lopes dos Santos, R. A., Prange, M., Castaneda, I. S., Schefuss, E., Mulitza, S., Schulz, M., et al. (2010). Glacial-interglacial variability in Atlantic meridional overturning circulation and thermocline adjustments in the tropical North Atlantic. *Earth and Planetary Science Letters*, *300*(3–4), 407–414. <https://doi.org/10.1016/j.epsl.2010.10.030>
- Lowenstein, T. K., Timofeeff, M. N., Brennan, S. T., Hardie, L. A., & Demicco, R. V. (2001). Oscillations in Phanerozoic seawater chemistry: Evidence from fluid inclusions. *Science*, *294*(5544), 1086–1088. <https://doi.org/10.1126/science.1064280>
- Makarova, M., Wright, J. D., Miller, K. G., Babila, T. L., Rosenthal, Y., & Park, J. I. (2017). Hydrographic and ecologic implications of foraminiferal stable isotopic response across the U.S. mid-Atlantic continental shelf during the Paleocene-Eocene Thermal Maximum. *Paleoceanography*, *32*, 56–73. <https://doi.org/10.1002/2016pa002985>
- Marchitto, T. M., Bryan, S. P., Curry, W. B., & McCorkle, D. C. (2007). Mg/Ca temperature calibration for the benthic foraminifer *Cibicides pachyderma*. *Paleoceanography*, *22*, Q03P21. <https://doi.org/10.1029/2006PA001287>
- Marchitto, T. M., Curry, W. B., Lynch-Stieglitz, J., Bryan, S. P., Cobb, K. M., & Lund, D. C. (2014). Improved oxygen isotope temperature calibrations for cosmopolitan benthic foraminifera. *Geochimica et Cosmochimica Acta*, *130*, 1–11. <https://doi.org/10.1016/j.gca.2013.12.034>
- Martin, P. A., Lea, D. W., Rosenthal, Y., Shackleton, N. J., Sarnthein, M., & Papenfuss, T. (2002). Quaternary deep sea temperature histories derived from benthic foraminiferal Mg/Ca. *Earth and Planetary Science Letters*, *198*(1–2), 193–209. [https://doi.org/10.1016/s0012-821x\(02\)00472-7](https://doi.org/10.1016/s0012-821x(02)00472-7)
- Meckler, A. N., Ziegler, M., Millán, M. I., Breitenbach, S. F. M., & Bernasconi, S. M. (2014). Long-term performance of the Kiel carbonate device with a new correction scheme for clumped isotope measurements. *Rapid Communications in Mass Spectrometry*, *28*(15), 1705–1715. <https://doi.org/10.1002/rcm.6949>
- Miller, K. G., Kominz, M. A., Browning, J. V., Wright, J. D., Mountain, G. S., Katz, M. E., et al. (2005). The Phanerozoic record of global sea-level change. *Science*, *310*(5752), 1293–1298. <https://doi.org/10.1126/science.1116412>
- Miller, K. G., Mountain, G. S., Browning, J. V., Kominz, M., Sugarman, P. J., Christie-Blick, N., et al. (1998). Cenozoic global sea level, sequences, and the New Jersey Transect: Results from coastal plain and continental slope drilling. *Reviews of Geophysics*, *36*(4), 569–601. <https://doi.org/10.1029/98RG01624>

- Miller, K. G., Sugarman, P. J., Browning, J. V., Olsson, R. K., Pekar, S. F., Reilly, T. J., et al. (1998). *Bass River site. Proceedings of the Ocean Drilling Program, initial reports, vol. 174AX*. College Station, TX: (Ocean Drilling Program). <https://doi.org/10.2973/odp.proc.ir.174ax.1998>
- Miller, K. G., Wright, J. D., & Fairbanks, R. G. (1991). Unlocking the ice house—Oligocene-Miocene oxygen isotopes, eustasy, and margin erosion. *Journal of Geophysical Research-Solid Earth and Planets*, *96*(B4), 6829–6848. <https://doi.org/10.1029/90JB02015>
- Müller, I. A., Fernandez, A., Radke, J., van Dijk, J., Bowen, D., Schwieters, J., & Bernasconi, S. M. (2017). Carbonate clumped isotope analyses with the long-integration dual-inlet (LIDI) workflow: Scratching at the lower sample weight boundaries. *Rapid Communications in Mass Spectrometry*, *31*(12), 1057–1066. <https://doi.org/10.1002/rcm.7878>
- Norris, R. D., Bice, K. L., Magno, E. A., & Wilson, P. A. (2002). Jiggling the tropical thermostat in the Cretaceous hothouse. *Geology*, *30*(4), 299–302. [https://doi.org/10.1130/0091-7613\(2002\)030<0299:jittit>2.0.co;2](https://doi.org/10.1130/0091-7613(2002)030<0299:jittit>2.0.co;2)
- Nürnberg, D., Bijma, J., & Hemleben, C. (1996). Assessing the reliability of magnesium in foraminiferal calcite as a proxy for water mass temperatures. *Geochimica et Cosmochimica Acta*, *60*(5), 803–814. [https://doi.org/10.1016/0016-7037\(95\)00446-7](https://doi.org/10.1016/0016-7037(95)00446-7)
- O'Brien, C. L., Robinson, S. A., Pancost, R. D., Sinninghe Damsté, J. S., Schouten, S., Lunt, D. J., et al. (2017). Cretaceous sea-surface temperature evolution: Constraints from TEX₈₆ and planktonic foraminiferal oxygen isotopes. *Earth-Science Reviews*, *172*, 224–247. <https://doi.org/10.1016/j.earscirev.2017.07.012>
- Olsson, R. K., Miller, K. G., Browning, J. V., Wright, J. D., & Cramer, B. S. (2002). Sequence stratigraphy and sea-level change across the Cretaceous-Tertiary boundary on the New Jersey passive margin. In C. Koeberl & K. G. MacLeod (Eds.), *Catastrophic events and mass extinctions: Impacts and beyond, Geological Society of America Special Paper 356* (pp. 97–108). Boulder, CO: Geological Society of America.
- Pearson, P. N., Ditchfield, P. W., Singano, J., Harcourt-Brown, K. G., Nicholas, C. J., Olsson, R. K., et al. (2001). Warm tropical sea surface temperatures in the Late Cretaceous and Eocene epochs. *Nature*, *413*, 481–487. <https://doi.org/10.1038/35097000>
- Pearson, P. N., van Dongen, B. E., Nicholas, C. J., Pancost, R. D., Schouten, S., Singano, J. M., & Wade, B. S. (2007). Stable warm tropical climate through the Eocene Epoch. *Geology*, *35*(3), 211–214. <https://doi.org/10.1130/g23175a.1>
- Peral, M., Daëron, M., Blamart, D., Bassinot, F., Dewilde, F., Smialkowski, N., et al. (2018). Updated calibration of the clumped isotope thermometer in planktonic and benthic foraminifera. *Geochimica Et Cosmochimica Acta*. <https://doi.org/10.1016/j.gca.2018.07.016>
- Peterse, F., Kim, J. H., Schouten, S., Kristensen, D. K., Koc, N., & Sinninghe Damsté, J. S. (2009). Constraints on the application of the MBT/CBT palaeothermometer at high latitude environments (Svalbard, Norway). *Organic Geochemistry*, *40*(6), 692–699. <https://doi.org/10.1016/j.orggeochem.2009.03.004>
- Peterse, F., van der Meer, J., Schouten, S., Weijers, J. W. H., Fierer, N., Jackson, R. B., et al. (2012). Revised calibration of the MBT-CBT paleotemperature proxy based on branched tetraether membrane lipids in surface soils. *Geochimica et Cosmochimica Acta*, *96*, 215–229. <https://doi.org/10.1016/j.gca.2012.08.011>
- Prahl, F. G., & Wakeham, S. G. (1987). Calibration of unsaturation patterns in long-chain ketone compositions for palaeotemperature assessment. *Nature*, *330*(6146), 367–369. <https://doi.org/10.1038/330367a0>
- Qian, P.-Y., Wang, Y., Lee, O. O., Lau, S. C. K., Yang, J. K., Lafi, F. F., et al. (2011). Vertical stratification of microbial communities in the Red Sea revealed by 16S rDNA pyrosequencing. *ISME Journal*, *5*(3), 507–518. <https://doi.org/10.1038/ismej.2010.112>
- Qin, W., Amin, S. A., Martens-Habben, W., Walker, C. B., Urakawa, H., Devol, A. H., et al. (2014). Marine ammonia-oxidizing archaeal isolates display obligate mixotrophy and wide ecotypic variation. *Proceedings of the National Academy of Sciences of the United States of America*, *111*(34), 12,504–12,509. <https://doi.org/10.1073/pnas.1324115111>
- Qin, W., Carlson, L. T., Armbrust, E. V., Devol, A. H., Moffett, J. W., Stahl, D. A., & Ingalls, A. E. (2015). Confounding effects of oxygen and temperature on the TEX₈₆ signature of marine Thaumarchaeota. *Proceedings of the National Academy of Sciences of the United States of America*, *112*(35), 10,979–10,984. <https://doi.org/10.1073/pnas.1501568112>
- Raitzsch, M., Dueñas-Bohórquez, A., Reichart, G.-J., de Nooijer, L. J., & Bickert, T. (2010). Incorporation of Mg and Sr in calcite of cultured benthic foraminifera: Impact of calcium concentration and associated calcite saturation state. *Biogeosciences*, *7*(3), 869–881. <https://doi.org/10.5194/bg-7-869-2010>
- Raitzsch, M., Kuhnert, H., Groeneveld, J., & Bickert, T. (2008). Benthic foraminifer Mg/Ca anomalies in South Atlantic core top sediments and their implications for paleothermometry. *Geochemistry Geophysics Geosystems*, *9*, Q05010. <https://doi.org/10.1029/2007GC001788>
- Rathburn, A. E., & DeDeckker, P. (1997). Magnesium and strontium compositions of recent benthic foraminifera from the Coral Sea, Australia and Prydz Bay, Antarctica. *Marine Micropaleontology*, *32*(3–4), 231–248. [https://doi.org/10.1016/s0377-8398\(97\)00028-5](https://doi.org/10.1016/s0377-8398(97)00028-5)
- Reichart, G.-J., Jorissen, F., Anschutz, P., & Mason, P. R. D. (2003). Single foraminiferal test chemistry records the marine environment. *Geology*, *31*(4), 355–358. [https://doi.org/10.1130/0091-7613\(2003\)031<0355:stfct>2.0.co;2](https://doi.org/10.1130/0091-7613(2003)031<0355:stfct>2.0.co;2)
- Rohling, E. J. (2007). Progress in paleosalinity: Overview and presentation of a new approach. *Paleoceanography*, *22*, PA3215. <https://doi.org/10.1029/2007PA001437>
- Rosenthal, Y., Boyle, E. A., & Slowey, N. (1997). Temperature control on the incorporation of magnesium, strontium, fluorine, and cadmium into benthic foraminiferal shells from Little Bahama Bank: Prospects for thermocline paleoceanography. *Geochimica et Cosmochimica Acta*, *61*(17), 3633–3643. [https://doi.org/10.1016/s0016-7037\(97\)00181-6](https://doi.org/10.1016/s0016-7037(97)00181-6)
- Rosenthal, Y., Lear, C. H., Oppo, D. W., & Linsley, B. K. (2006). Temperature and carbonate ion effects on Mg/Ca and Sr/Ca ratios in benthic foraminifera: Aragonitic species *Hoeglundina elegans*. *Paleoceanography*, *21*, PA1007. <https://doi.org/10.1029/2005PA001158>
- Russell, A. D., Honisch, B., Spero, H. J., & Lea, D. W. (2004). Effects of seawater carbonate ion concentration and temperature on shell U, Mg, and Sr in cultured planktonic foraminifera. *Geochimica et Cosmochimica Acta*, *68*(21), 4347–4361. <https://doi.org/10.1016/j.gca.2004.03.013>
- Schlitzer, R., 2015. Ocean Data View, odv.awi.de.
- Schouten, S., Hopmans, E. C., Schefuss, E., & Sinninghe Damsté, J. S. (2002). Distributional variations in marine crenarchaeotal membrane lipids: A new tool for reconstructing ancient sea water temperatures? *Earth and Planetary Science Letters*, *204*(1–2), 265–274. [https://doi.org/10.1016/s0012-821x\(02\)00979-2](https://doi.org/10.1016/s0012-821x(02)00979-2)
- Schouten, S., Hopmans, E. C., & Sinninghe Damsté, J. S. (2013). The organic geochemistry of glycerol dialkyl glycerol tetraether lipids: A review. *Organic Geochemistry*, *54*, 19–61. <https://doi.org/10.1016/j.orggeochem.2012.09.006>
- Schrag, D. P., DePaolo, D. J., & Richter, F. M. (1995). Reconstructing past sea surface temperatures: Correcting for diagenesis of bulk marine carbonate. *Geochimica et Cosmochimica Acta*, *59*(11), 2265–2278. [https://doi.org/10.1016/0016-7037\(95\)00105-9](https://doi.org/10.1016/0016-7037(95)00105-9)
- Segev, E., & Erez, J. (2006). Effect of Mg/Ca ratio in seawater on shell composition in shallow benthic foraminifera. *Geochemistry Geophysics Geosystems*, *7*, Q02P09. <https://doi.org/10.1029/2005GC000969>

- Shackleton, N. J., & Kennett, J. P. (1975). Paleotemperature history of the Cenozoic and the initiation of Antarctic glaciation: oxygen and carbon isotope analyses in DSDP Sites 277, 279, and 281. *Initial Report Deep Sea Drilling Project, 29*, 743–755. <https://doi.org/10.2973/dsdp.proc.29.117.1975>
- van Sickele, W. A., Kominz, M. A., Miller, K. G., & Browning, J. V. (2004). Late Cretaceous and Cenozoic sea-level estimates: Backstripping analysis of borehole data, onshore New Jersey. *Basin Research, 16*(4), 451–465. <https://doi.org/10.1111/j.1365-2117.2004.00242.x>
- Sinninghe Damsté, J. S. (2016). Spatial heterogeneity of sources of branched tetraethers in shelf systems: The geochemistry of tetraethers in the Berau River delta (Kalimantan, Indonesia). *Geochimica et Cosmochimica Acta, 186*, 13–31. <https://doi.org/10.1016/j.gca.2016.04.033>
- Sinninghe Damsté, J. S., Ossebaar, J., Schouten, S., & Verschuren, D. (2012). Distribution of tetraether lipids in the 25-ka sedimentary record of Lake Challa: Extracting reliable TEX₈₆ and MBT/CBT palaeotemperatures from an equatorial African lake. *Quaternary Science Reviews, 50*, 43–54. <https://doi.org/10.1016/j.quascirev.2012.07.001>
- Sluijs, A., & Brinkhuis, H. (2009). A dynamic climate and ecosystem state during the Paleocene-Eocene thermal maximum: Inferences from dinoflagellate cyst assemblages on the New Jersey Shelf. *Biogeosciences, 6*(8), 1755–1781. <https://doi.org/10.5194/bg-6-1755-2009>
- Sluijs, A., Brinkhuis, H., Crouch, E. M., John, C. M., Handley, L., Munsterman, D., et al. (2008). Eustatic variations during the Paleocene-Eocene greenhouse world. *Paleoceanography, 23*, PA4216. <https://doi.org/10.1029/2008PA001615>
- Sluijs, A., Brinkhuis, H., Schouten, S., Bohaty, S. M., John, C. M., Zachos, J. C., et al. (2007). Environmental precursors to rapid light carbon injection at the Palaeocene/Eocene boundary. *Nature, 450*(7173), 1218–1221. <https://doi.org/10.1038/nature06400>
- Sluijs, A., van Roij, L., Harrington, G. J., Schouten, S., Sessa, J. A., Levay, L. J., et al. (2014). Warming, euxinia and sea level rise during the Paleocene-Eocene thermal maximum on the Gulf Coastal Plain: Implications for ocean oxygenation and nutrient cycling. *Climate of the Past, 10*(4), 1421–1439. <https://doi.org/10.5194/cp-10-1421-2014>
- Snell, K. E., Thrasher, B. L., Eiler, J. M., Koch, P. L., Sloan, L. C., & Tabor, N. J. (2013). Hot summers in the Bighorn Basin during the early Paleogene. *Geology, 41*(1), 55–58. <https://doi.org/10.1130/g33567.1>
- Stanley, S. M., & Hardie, L. A. (1998). Secular oscillations in the carbonate mineralogy of reef-building and sediment-producing organisms driven by tectonically forced shifts in seawater chemistry. *Palaeogeography Palaeoclimatology Palaeoecology, 144*(1–2), 3–19. [https://doi.org/10.1016/s0031-0182\(98\)00109-6](https://doi.org/10.1016/s0031-0182(98)00109-6)
- Steuber, T., & Veizer, J. (2002). Phanerozoic record of plate tectonic control of seawater chemistry and carbonate sedimentation. *Geology, 30*(12), 1123–1126. [https://doi.org/10.1130/0091-7613\(2002\)030<1123:proptc>2.0.co;2](https://doi.org/10.1130/0091-7613(2002)030<1123:proptc>2.0.co;2)
- Sugarman, P. J., Miller, K. G., Olsson, R. K., Browning, J. V., Wright, J. D., de Romero, L., et al. (1999). The Cenomanian/Turonian carbon burial event, Bass River, NJ, USA; geochemical, paleoecological, and sea-level changes. (1999). *Journal of Foraminiferal Research, 29*(4), 438–452.
- Tierney, J. E. (2014). 12.14—Biomarker-based inferences of past climate: The TEX₈₆ Paleotemperature proxy A2—Holland, Heinrich D. In K. K. Turekian (Ed.), *Treatise on geochemistry*, (Second ed. pp. 379–393). Oxford: Elsevier.
- Tierney, J. E., & Tingley, M. P. (2014). A Bayesian, spatially-varying calibration model for the TEX₈₆ proxy. *Geochimica et Cosmochimica Acta, 127*, 83–106. <https://doi.org/10.1016/j.gca.2013.11.026>
- Tierney, J. E., & Tingley, M. P. (2015). A TEX₈₆ surface sediment database and extended Bayesian calibration. *Scientific Data, 2*, 150029. <https://doi.org/10.1038/sdata.2015.29>
- Tierney, J. E., & Tingley, M. P. (2018). BAYSPLINE: A new calibration for the Alkenone paleothermometer. *Paleoceanography and Paleoclimatology, 33*, 281–301. <https://doi.org/10.1002/2017pa003201>
- Tisserand, A. A., Dokken, T. M., Waelbroeck, C., Gherardi, J. M., Scao, V., Fontanier, C., & Jorissen, F. (2013). Refining benthic foraminiferal Mg/Ca-temperature calibrations using core-tops from the western tropical Atlantic: Implication for paleotemperature estimation. *Geochemistry Geophysics Geosystems, 14*, 929–946. <https://doi.org/10.1002/ggge.20043>
- Trommer, G., Siccha, M., van der Meer, M. T. J., Schouten, S., Sinninghe Damsté, J. S., Schulz, H., et al. (2009). Distribution of Crenarchaeota tetraether membrane lipids in surface sediments from the Red Sea. *Organic Geochemistry, 40*(6), 724–731. <https://doi.org/10.1016/j.orggeochem.2009.03.001>
- van Helmond, N. A. G. M., Sluijs, A., Papadomanolaki, N. M., Plint, A. G., Grocke, D. R., Pearce, M. A., et al. (2016). Equatorward phytoplankton migration during a cold spell within the Late Cretaceous super-greenhouse. *Biogeosciences, 13*(9), 2859–2872. <https://doi.org/10.5194/bg-13-2859-2016>
- van Helmond, N. A. G. M., Sluijs, A., Reichert, G.-J., Sinninghe Damsté, J. S., Slomp, C. P., & Brinkhuis, H. (2014). A perturbed hydrological cycle during Oceanic Anoxic Event 2. *Geology, 42*(2), 123–126. <https://doi.org/10.1130/g34929.1>
- Vellekoop, J., Esmeray-Senlet, S., Miller, K. G., Browning, J. V., Sluijs, A., van de Schootbrugge, B., et al. (2016). Evidence for Cretaceous-Paleogene boundary bolide “impact winter” conditions from New Jersey, USA. *Geology, 44*(8), 619–622. <https://doi.org/10.1130/G37961.1>
- Volkman, J. K., Barrett, S. M., Blackburn, S. I., & Sikes, E. L. (1995). Alkenones in *Gephyrocapsa Oceanica*: Implications for studies of paleoclimate. *Geochimica et Cosmochimica Acta, 59*(3), 513–520. [https://doi.org/10.1016/0016-7037\(95\)00325-t](https://doi.org/10.1016/0016-7037(95)00325-t)
- Weijers, J. W. H., Schouten, S., Sluijs, A., Brinkhuis, H., & Sinninghe Damsté, J. S. (2007). Warm arctic continents during the Palaeocene-Eocene thermal maximum. *Earth and Planetary Science Letters, 261*(1–2), 230–238. <https://doi.org/10.1016/j.epsl.2007.06.033>
- Weijers, J. W. H., Schouten, S., Spaargaren, O. C., & Sinninghe Damsté, J. S. (2006). Occurrence and distribution of tetraether membrane lipids in soils: Implications for the use of the TEX₈₆ proxy and the BIT index. *Organic Geochemistry, 37*(12), 1680–1693. <https://doi.org/10.1016/j.orggeochem.2006.07.018>
- Weijers, J. W. H., Schouten, S., van den Donker, J. C., Hopmans, E. C., & Sinninghe Damsté, J. S. (2007). Environmental controls on bacterial tetraether membrane lipid distribution in soils. *Geochimica et Cosmochimica Acta, 71*(3), 703–713. <https://doi.org/10.1016/j.gca.2006.10.003>
- Wendler, I., Huber, B. T., MacLeod, K. G., & Wendler, J. E. (2013). Stable oxygen and carbon isotope systematics of exquisitely preserved Turonian foraminifera from Tanzania—Understanding isotopic signatures in fossils. *Marine Micropaleontology, 102*, 1–33. <https://doi.org/10.1016/j.marmicro.2013.04.003>
- Wilkinson, B. H., & Algeo, T. J. (1989). Sedimentary carbonate record of calcium-magnesium cycling. *American Journal of Science, 289*(10), 1158–1194. <https://doi.org/10.2475/ajs.289.10.1158>
- Wing, S. L., Harrington, G. J., Smith, F. A., Bloch, J. I., Boyer, D. M., & Freeman, K. H. (2005). Transient floral change and rapid global warming at the Paleocene-Eocene boundary. *Science, 310*(5750), 993–996. <https://doi.org/10.1126/science.1116913>
- Wit, J. C., de Nooijer, L. J., Haig, J., Jorissen, F. J., Thomas, E., & Reichert, G. J. (2017). Towards reconstructing ancient seawater Mg/Ca by combining porcelaneous and hyaline foraminiferal Mg/Ca-temperature calibrations. *Geochimica et Cosmochimica Acta, 211*, 341–354. <https://doi.org/10.1016/j.gca.2017.05.036>

- Wuchter, C., Schouten, S., Coolen, M. J. L., & Sinninghe Damsté, J. S. (2004). Temperature-dependent variation in the distribution of tetraether membrane lipids of marine Crenarchaeota: Implications for TEX₈₆ paleothermometry. *Paleoceanography*, *19*, PA4028. <https://doi.org/10.1029/2004PA001041>
- Yu, J. M., & Elderfield, H. (2008). Mg/Ca in the benthic foraminifera *Cibicides wuellerstorfi* and *Cibicides mundulus*: Temperature versus carbonate ion saturation. *Earth and Planetary Science Letters*, *276*(1–2), 129–139. <https://doi.org/10.1016/j.epsl.2008.09.015>
- Zachos, J. C., Dickens, G. R., & Zeebe, R. E. (2008). An early Cenozoic perspective on greenhouse warming and carbon-cycle dynamics. *Nature*, *451*(7176), 279–283. <https://doi.org/10.1038/nature06588>
- Zachos, J. C., Schouten, S., Bohaty, S., Quattlebaum, T., Sluijs, A., Brinkhuis, H., et al. (2006). Extreme warming of mid-latitude coastal ocean during the Paleocene-Eocene thermal maximum: Inferences from TEX₈₆ and isotope data. *Geology*, *34*(9), 737–740. <https://doi.org/10.1130/g22522.1>
- Zachos, J. C., Stott, L. D., & Lohmann, K. C. (1994). Evolution of early Cenozoic marine temperatures. *Paleoceanography*, *9*(2), 353–387. <https://doi.org/10.1029/93PA03266>
- Zhang, Y. G., & Liu, X. (2018). Export depth of the TEX₈₆ signal. *Paleoceanography and Paleoclimatology*, *33*, 666–671. <https://doi.org/10.1029/2018PA003337>
- Zhang, Y. G., Pagani, M., & Wang, Z. (2016). Ring index: A new strategy to evaluate the integrity of TEX₈₆ paleothermometry. *Paleoceanography*, *31*, 220–232. <https://doi.org/10.1002/2015pa002848>
- Zhang, Y. G., Zhang, C. L., Liu, X.-L., Li, L., Hinrichs, K.-U., & Noakes, J. E. (2011). Methane index: A tetraether archaeal lipid biomarker indicator for detecting the instability of marine gas hydrates. *Earth and Planetary Science Letters*, *307*(3), 525–534. <https://doi.org/10.1016/j.epsl.2011.05.031>

References From the Supporting Information

- Bernasconi, S. M., Hu, B., Wacker, U., Fiebig, J., Breitenbach, S. F. M., & Rutz, T. (2013). Background effects on Faraday collectors in gas-source mass spectrometry and implications for clumped isotope measurements. *Rapid Communications in Mass Spectrometry*, *27*(5), 603–612. <https://doi.org/10.1002/rcm.6490>
- Dennis, K. J., Affek, H. P., Passey, B. H., Schrag, D. P., & Eiler, J. M. (2011). Defining an absolute reference frame for ‘clumped’ isotope studies of CO₂. *Geochimica Et Cosmochimica Acta*, *75*(22), 7117–7131. <https://doi.org/10.1016/j.gca.2011.09.025>
- Dueñas-Bohórquez, A., da Rocha, R. E., Kuroyanagi, A., de Nooijer, L. J., Bijma, J., & Reichart, G.-J. (2011). Interindividual variability and ontogenetic effects on Mg and Sr incorporation in the planktonic foraminifer *Globigerinoides sacculifer*. *Geochimica et Cosmochimica Acta*, *75*(2), 520–532. <https://doi.org/10.1016/j.gca.2010.10.006>
- Grauel, A.-L., Schmid, T. W., Hu, B., Bergami, C., Capotondi, L., Zhou, L., & Bernasconi, S. M. (2013). Calibration and application of the ‘clumped isotope’ thermometer for foraminifera for high-resolution climate reconstructions. *Geochimica et Cosmochimica Acta*, *108*, 125–140. <https://doi.org/10.1016/j.gca.2012.12.049>
- Hathorne, E. C., James, R. H., Savage, P., & Alard, O. (2008). Physical and chemical characteristics of particles produced by laser ablation of biogenic calcium carbonate. *Journal of Analytical Atomic Spectrometry*, *23*(2), 240–243. <https://doi.org/10.1039/b706727e>
- Henkes, G. A., Passey, B. H., Wanamaker, A. D. Jr., Grossman, E. L., Ambrose, W. G. Jr., & Carroll, M. L. (2013). Carbonate clumped isotope compositions of modern marine mollusk and brachiopod shells. *Geochimica et Cosmochimica Acta*, *106*, 307–325. <https://doi.org/10.1016/j.gca.2012.12.020>
- Hopmans, E. C., Schouten, S., Pancost, R. D., van der Meer, M. T. J., & Sinninghe Damsté, J. S. (2000). Analysis of intact tetraether lipids in archaeological cell material and sediments by high performance liquid chromatography/atmospheric pressure chemical ionization mass spectrometry. *Rapid Communications in Mass Spectrometry*, *14*(7), 585–589. [https://doi.org/10.1002/\(sici\)1097-0231\(20000415\)14:7<585::aid-rcm913>3.3.co;2-e](https://doi.org/10.1002/(sici)1097-0231(20000415)14:7<585::aid-rcm913>3.3.co;2-e)
- Hopmans, E. C., Schouten, S., & Sinninghe Damsté, J. S. (2016). The effect of improved chromatography on GDGT-based palaeoproxies. *Organic Geochemistry*, *93*, 1–6. <https://doi.org/10.1016/j.orggeochem.2015.12.006>
- Huntington, K. W., Eiler, J. M., Affek, H. P., Guo, W., Bonifacie, M., Yeung, L. Y., et al. (2009). Methods and limitations of ‘clumped’ CO₂ isotope (Δ₄₇) analysis by gas-source isotope ratio mass spectrometry. *Journal of Mass Spectrometry*, *44*(9), 1318–1329. <https://doi.org/10.1002/jms.1614>
- Jochum, K. P., Weis, U., Stoll, B., Kuzmin, D., Yang, Q. C., Raczek, I., et al. (2011). Determination of reference values for NIST SRM 610-617 glasses following ISO guidelines. *Geostandards and Geoanalytical Research*, *35*(4), 397–429. <https://doi.org/10.1111/j.1751-908X.2011.00120.x>
- Reinhardt, E. G., Cavazza, W., Patterson, R. T., & Blenkinsop, J. (2000). Differential diagenesis of sedimentary components and the implication for strontium isotope analysis of carbonate rocks. *Chemical Geology*, *164*(3–4), 331–343. [https://doi.org/10.1016/s0009-2541\(99\)00147-3](https://doi.org/10.1016/s0009-2541(99)00147-3)
- Schouten, S., Hugué, C., Hopmans, E. C., Kienhuis, M. V. M., & Sinninghe Damsté, J. S. (2007). Analytical methodology for TEX₈₆ paleothermometry by high-performance liquid chromatography/atmospheric pressure chemical ionization-mass spectrometry. *Analytical Chemistry*, *79*(7), 2940–2944. <https://doi.org/10.1021/ac062339v>
- Thornalley, D. J. R., Bauch, H. A., Gebbie, G., Guo, W., Ziegler, M., Bernasconi, S. M., et al. (2015). A warm and poorly ventilated deep Arctic Mediterranean during the last glacial period. *Science*, *349*(6249), 706–710. <https://doi.org/10.1126/science.aaa9554>